




Paleocene metamorphism along the Pennine–Austroalpine suture constrained by U–Pb dating of titanite and rutile (Malenco, Alps)

Suzanne M. Picazo¹ · Tanya A. Ewing^{1,2}  · Othmar Müntener¹

Received: 12 February 2019 / Accepted: 18 August 2019 / Published online: 13 September 2019
© The Author(s) 2019

Abstract

We present in situ rutile and titanite U–Pb geochronology for three samples from the Ur breccia, which forms the boundary between the Malenco unit and the Margna nappe (Eastern Central Alps) near Pass d’Ur in southeast Switzerland. These samples both oceanic brecciated material and a blackwall reaction zone in contact with a micaschist and serpentized peridotite. Peak temperatures during Alpine metamorphism in these units were $\sim 460 \pm 30$ °C. Textural observations combined with new geochronological data indicate that rutile and titanite both grew below their closure temperatures during Alpine metamorphism. We present a technique to calculate the most precise and accurate ages possible using a two-dimensional U–Pb isochron on a Wetherill concordia. Rutile from two samples gave a U–Pb isochron age of 63.0 ± 3.0 Ma. This age conflicts with previous ^{39}Ar – ^{40}Ar data on heterogeneous amphiboles from which an age of 90–80 Ma was inferred for the high pressure part of the Alpine evolution, but is consistent with K–Ar ages and Ar–Ar ages on phengitic white mica. Titanite from three samples gave a U–Pb isochron age of 54.7 ± 4.1 Ma. This age is consistent with Rb–Sr isochron ages on mylonites along and in the footwall of the Lunghin–Mortirolo movement zone, a major boundary that separates ductile deformation in the footwall from mostly localized and brittle deformation in the hangingwall. Our ages indicate a Paleocene rather than upper Cretaceous metamorphism of the Pennine–Austroalpine boundary and permit at most ~ 15 Myr, and possibly much less, between the growth of rutile and titanite.

Keywords U–Pb geochronology · Rutile · Titanite · Isochron · TZARS reaction · Malenco–Margna nappes

1 Introduction

U–Pb geochronology is well established as the ‘gold standard’ of dating techniques, and has most frequently been applied to the extremely robust mineral zircon (e.g. Rubatto 2017). In the past decade, U–Pb geochronology of other accessory minerals has attracted increasing interest,

with the growing recognition that in metamorphic contexts they may record a different part of the P–T evolution from zircon (e.g. Engi 2017; Kohn 2017; Zack and Kooijman 2017). However, U–Pb dating of moderate- to low-temperature metamorphic overprints or retrogression is notoriously difficult (e.g. Rasmussen et al. 2001). At such temperatures, the U–Pb systematics of many minerals are not reset or only partially reset—and newly-grown minerals tend to be low in U and thus difficult to date. For other geochronological systems such as Rb–Sr and K–Ar, the assumption of isotopic equilibrium at the sample scale, which underpins these methods, is increasingly difficult to justify at low temperatures, and under such conditions these techniques often yield excessively scattered data from which robust ages cannot be determined (e.g. Bachmann et al. 2009).

An appealing approach to date moderate temperature metamorphism is to U–Pb date newly-formed minerals that grew below their closure temperature. In this case the mineral will record growth rather than cooling ages and

Editorial Handling: E. Gnoss.

Electronic supplementary material The online version of this article (<https://doi.org/10.1007/s00015-019-00346-1>) contains supplementary material, which is available to authorized users.

✉ Tanya A. Ewing
tanya.ewing@geo.unibe.ch

¹ Institute of Earth Sciences, University of Lausanne,
1015 Lausanne, Switzerland

² Present Address: Institute of Geological Sciences, University
of Bern, Balzerstrasse 1+3, 3012 Bern, Switzerland

complications regarding knowledge of the closure temperature or incomplete equilibration are removed, but low U contents are a common challenge. In this study we explore the potential of in situ U–Pb dating of low-U rutile and titanite formed at < 500 °C to obtain growth ages that can be directly related to moderate-temperature metamorphism. This approach requires that there is clear textural evidence to link the mineral growth to specific reactions and/or parts of the pressure–temperature evolution. A common example is titanite rims formed at the expense of rutile, which record a typical decompression reaction during exhumation and retrograde metamorphic evolution (e.g. Lucassen et al. 2010; Cruz-Uribe et al. 2014). While this is a commonly reported texture, with a clear interest for dating (Zack et al. 2010), there is a dearth of successful attempts to U–Pb date both rutile and titanite in such a textural relationship and from the same sample. Dating accessory minerals in such an overgrowth relationship demands in situ analysis: while TIMS analysis is more precise, it requires the dissolution of whole grains, which in the case of titanite rimming rutile would provide a meaningless average of U and Pb from the two minerals. In this contribution we present LA-ICPMS U–Pb geochronology of rutile and titanite with an overgrowth relationship from samples from the Eastern Central Alps. We show that both minerals record growth ages that date two different points in the P–T evolution during the Alpine orogeny, providing important new constraints on the timing of the metamorphic evolution of the Pennine–Austroalpine boundary.

2 Geodynamic context

The European Alps are one of the most classic examples of orogenesis. They experienced a complex, polyphase compressional history, which was the result of continent–continent collision following the closure of the Alpine Tethys Ocean. Age constraints on the different phases of Alpine deformation are crucial to our understanding of how orogeny proceeded and on what timescales. However, obtaining robust geochronological constraints that can be related to Alpine events can be challenging, owing to a paucity of geochronometers that both record appropriate conditions and provide robust ages. Interpretation of geochronological data for the Alpine orogeny is further complicated by its polymetamorphic nature, and potential inheritance. The Alpine Tethys had a polyphase history, starting in late Triassic and Early Jurassic with rifting and thinning of the continental crust, mantle exhumation and formation of oceanic lithosphere (e.g. Lemoine and Trümpy 1987; Froitzheim and Eberli 1990; Manatschal and Müntener 2009; Mohn et al. 2010). While the extent and nature of oceanic crust is a matter of debate (e.g. Picazo

et al. 2016), ocean closure occurred progressively starting in the late Cretaceous and eventually lead to Eocene continental collision (Froitzheim and Manatschal 1996; Schmid et al. 2004).

Following passive margin formation, the opening ocean separated the European plate from the Adriatic plate, and continental lithospheric mantle was exhumed to the seafloor leading to alteration by hydrothermal fluid circulation and locally, to near-seafloor brecciation processes. During subduction, oceanic units and parts of the European plate were subducted below the Adriatic plate and later exhumed. The juxtaposition of passive margin and associated ophiolitic units along the Pennine–Austroalpine boundary occurred in two orogenic cycles including thrusting followed by extensional overprint (e.g. Froitzheim et al. 1994; Handy et al. 1996; Mohn et al. 2011). The first cycle is mid to upper Cretaceous in age and is expressed by imbricate thrusting and folding, followed by extension along several shear zones (e.g. Froitzheim et al. 1994). The most prominent of these shear zones is the Lunghin–Mortirolo movement zone, which juxtaposes weakly metamorphic Austroalpine units against the strongly deformed and metamorphosed Margna–Sella and Malenco units (Mohn et al. 2011). The Austroalpine and upper Penninic units were juxtaposed against the middle Penninic (European) units in the Eocene–Oligocene, expressed by N–S shortening with gently E-dipping fold axes followed by orogen-parallel E–W extension (Turba mylonite phase) that is truncated by the Oligocene Bergell intrusion (e.g. Nievergelt et al. 1996). Despite several attempts to date Alpine metamorphism in the Eastern Central Alps, it has been difficult to precisely constrain the timing of Alpine events from the highly scattered data (e.g. Hunziker et al. 1992; Handy et al. 1996; Villa et al. 2000; Price et al. 2018).

Here we present U–Pb ages for rutile and overgrowing titanite rims from the footwall of the Lunghin–Mortirolo movement zone along the contact of the highly deformed Margna–Sella and Malenco units. We argue that both minerals formed below their closure temperature during the Alpine orogeny, and thus record growth ages during Alpine convergence. These are the first U–Pb ages determined for rutile and titanite from Alpine parageneses in this region, and provide novel geochronological constraints for Alpine metamorphism in the Eastern Central Alps. We show that it is possible to obtain robust U–Pb ages for young (Paleocene), relatively low-U titanite by using a 2-D isochron approach on a Wetherill concordia. This slightly modified approach is a valuable tool for dating low-grade, young metamorphic events.

3 Geological setting of the Val Malenco region

The Val Malenco exposes parts of the suture zone between the Penninic and the Austroalpine domains. The Margna nappe belongs to the Lower Austroalpine nappe system (LAA; Mohn et al. 2011) and is a composite basement containing pre-rift lower crustal rocks (gabbros and granulite facies metapelites), upper crustal intrusions (Spillmann and Büchi 1993) covered by a Mesozoic sedimentary sequence derived from the former distal Adriatic margin (Trommsdorff et al. 1993). The Malenco unit belongs to the Upper Penninic nappes and is made of Permian granulite facies lower crust, a gabbroic intrusion and ultramafic rocks that represent contiguous Permian subcontinental mantle (Müntener and Hermann 1996). During Jurassic extension of the Piemonte domain, the Malenco peridotites were exhumed to the seafloor (at 170–140 Ma; Müntener et al. 2000) and affected by different near-seafloor alteration processes (serpentinization and carbonation) leading to sedimentary ophicarbonates (Hermann and Müntener 1996) as also described in other Alpine ophiolites (e.g. Ventina, NW Malenco, Pozzorini 1996; Totalp, Picazo et al. 2013 and references therein).

The Alpine metamorphic conditions during the upper Cretaceous reached 0.4–0.7 GPa and temperatures of ~ 450 °C (Guntli and Liniger 1989; Mellini et al. 1987; Benning and Sidler 1992). Regional metamorphism is later overprinted by the Oligocene Bergell intrusion, which formed a well-known contact aureole (Trommsdorff and Evans 1972). The timing of metamorphism associated with the Alpine orogeny in Val Malenco is poorly constrained. Amphibole Ar–Ar data from mafic rocks were interpreted to record a high-pressure event at 91–83 Ma and a thermal maximum at 73–67 Ma (Villa et al. 2000). However, these Ar–Ar amphibole ages are the result of a deconvolution of multiple generations of amphiboles from complex Ar–Ar spectra, and therefore open to considerable uncertainties.

The interface between the Margna and Malenco nappes is a tectonic contact locally characterized by breccias with ultramafic and basement clasts, and carbonated serpentinites (Montrasio et al. 2005). These breccias are exceptionally well exposed in the Pass d'Ur region at the border between Switzerland and Italy (Montrasio et al. 2005 and Fig. 1). Breccias reworking ultramafic and/or continental rocks with sedimentary rocks are well known in the Western and Central Alps (e.g. Masini et al. 2012; Beltrando et al. 2014; Masson et al. 2008). However, the processes by which such breccias form is still a matter of debate. Two explanations have been proposed to explain the formation of such breccias at the interface between continental and mantle units: (a) tectono-sedimentary brecciation and

alteration during the Jurassic rifting phase (Masini et al. 2012; Beltrando et al. 2014), similar to drilled breccias of the Iberia-Newfoundland margin; or (b) reworking of rocks along a 'subduction interface' during the Alpine orogeny (e.g. Locatelli et al. 2018).

In this study we focus on the Pass d'Ur region in East-Malenco, near Poschiavo in SE-Switzerland (Fig. 1). There, the Margna nappe is either directly in contact with serpentinitized peridotites or in contact with a breccia containing cm- to dm-sized clasts embedded in chlorite-micaschists. Ultramafic rocks of the Malenco unit are highly serpentinitized and well-exposed over more than 15 km² (Montrasio et al. 2005). At Pass d'Ur, up to 200 m² of brecciated material is exposed at the interface between the ultramafic rocks of the Malenco unit and the continental rocks of the Margna nappe. The breccia clasts are made of metasomatized ultramafic rocks and paragneisses similar to the Margna crystalline rocks (Sidler and Benning 1992). The chlorite-micaschists observed at the contact between ultramafic and mafic rocks consist predominantly of amphibole, chlorite and phlogopite and are interpreted as blackwall rocks resulting from chemical gradients and diffusive mass-transfer of elements between ultramafic bodies and quartzofeldspathic rocks (e.g. Frost 1975).

In the breccia from Pass d'Ur, Sidler and Benning (1992) described titanite aligned in the main Alpine foliation. They proposed that titanite formed at the expense of rutile during Alpine metamorphism, based on the observation that rutile was found included in titanite and albite porphyroblasts, but only titanite was found in the matrix. Titanite and rutile are therefore an ideal target to provide new geochronological constraints on the timing of Alpine metamorphism.

4 Methodology

4.1 Sample preparation and imaging

Each sample was thin sectioned, then crushed to < 200 µm. Rutile and titanite were separated using standard heavy liquid and magnetic techniques, then hand-picked and mounted in 2.5 cm epoxy discs, which were polished to expose the mid-section of grains for analysis. Rutile and titanite in grain mounts were imaged in reflected and transmitted light using a petrographic microscope. Titanite and rutile were imaged by backscattered electrons (BSE) to identify zoning, inclusions or alteration, and rutile remnants. BSE imaging was carried out on a Tescan Mira II LMU Scanning Electron Microprobe (SEM) at the University of Lausanne, with operating conditions at an acceleration voltage of 20 kV, a probe current of 0.2–0.4 nA, and 8 mm working distance.

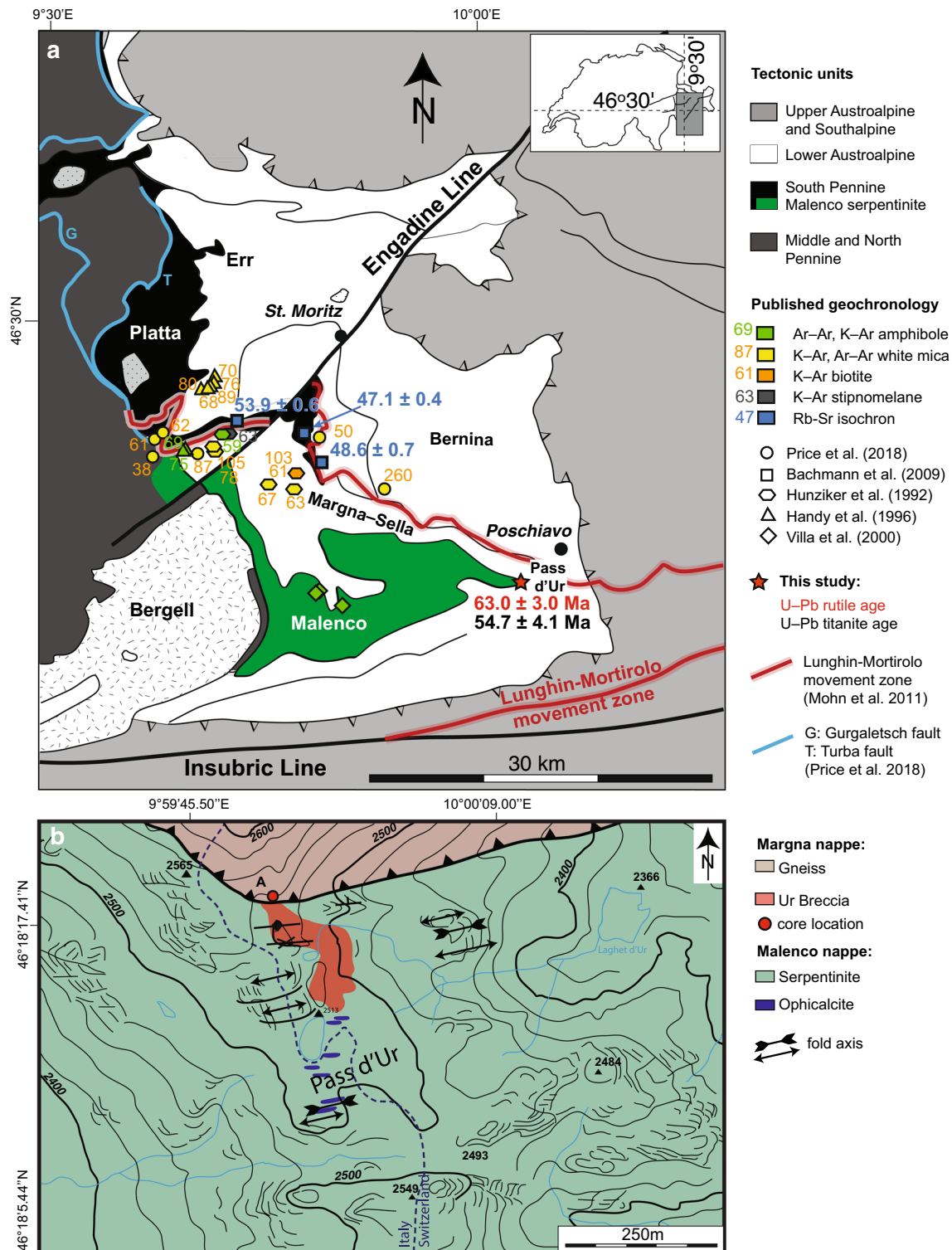


Fig. 1 **a** Tectonic map showing location of the Malenco unit and Margna–Sella nappes and the surrounding Austroalpine and South Penninic nappes, in the SE of Switzerland and northern Italy. The Malenco unit is located below the Lunghin–Mortiolo movement zone (Mohn et al. 2011). The location and ages of geochronological data from literature is provided; we distinguish authors (shape; Hunziker et al. 1992; Handy et al. 1996; Bachmann et al. 2009; Price

et al. 2018), from geochronological methods (colour). The red star shows emplacement of studied area. **b** The brecciated material is in red, at the boundary between the Margna and Malenco nappes. The entire region is folded and the mantle outcrops as a tectonic window. Locally opicalcites in Malenco serpentinitized peridotites attest that these rocks cropped out at the seafloor before Alpine deformation

4.2 Major and trace element analysis (LA-ICPMS)

Major and trace elements were measured by laser ablation inductively coupled plasma mass spectrometry (LA-ICPMS) on an Element XR sector field ICPMS coupled to a New Wave UP-193FX Excimer laser ablation system at the University of Lausanne. For both rutile and titanite, concentrations were calculated relative to the primary standard SRM612, using the reference values of Jochum et al. (2011).

Rutile and titanite were analysed with a beam size of 38 or 50 μm , with an on-sample energy density of 6 J/cm^2 and repetition rate of 10 Hz. For rutile, 26 elements were measured in peak-hopping mode. TiO_2 was used as an internal standard, assuming a stoichiometric concentration of 100 wt%. For titanite, 35 elements were measured in peak-hopping mode. CaO was used as an internal standard, assuming a stoichiometric concentration of 28.6 wt%. The validity of the values used for internal standardisation for rutile and titanite was confirmed for each analysis by summing the concentration of all measured elements recalculated as oxides. If rutile or titanite had a significantly non-stoichiometric composition, i.e. high concentrations of non-essential elements, this would be detected as totals that deviated significantly from 100 wt%. This was not the case, with all analyses giving totals close to 100 wt%.

4.3 U–Pb geochronology

U–Pb isotope ratios were determined by LA-ICPMS using the same instrumentation as geochemical analyses, but were measured in separate sessions and with different operating conditions. Prior to analysis, mounts were cleaned with 5% HNO_3 and ethanol. The instrument was tuned on NIST-612 synthetic glass for maximum sensitivity while minimising mass bias and production of doubly-charged ions and oxides. Dead time on our instrument is measured and updated each time that the voltage on the detector is changed. U–Pb data were processed using Iolite 3.65 and the VizualAge_UcomPbine Data Reduction Scheme (Chew et al. 2014; Paton et al. 2010, 2011). This allows for correction of common Pb in the primary standard, prior to using it to calibrate unknown ages, which is critical for accurate calibration in common Pb bearing minerals (Chew et al. 2014). Although ^{235}U was measured, the measured values were not used for calculation of isotope ratios, and ^{235}U was instead calculated from the measured ^{238}U by VizualAge_UcomPbine. A $^{238}\text{U}/^{235}\text{U}$ of 137.818 (Hiess et al. 2012) was used for this calculation. Although titanite is one of the few minerals that has shown variability in $^{238}\text{U}/^{235}\text{U}$ outside the canonical range of

137.818 ± 0.045 for the bulk Earth (Hiess et al. 2012), this level of variation would have no effect on our calculated ages. We tested this by processing our titanite U–Pb data using the highest and lowest $^{238}\text{U}/^{235}\text{U}$ reported by Hiess et al. (2012) for titanite, as well as the canonical value of 137.818 ± 0.045 based on zircon and other minerals, using the VizualAge data reduction scheme (which allows the user to specify a $^{238}\text{U}/^{235}\text{U}$; Petrus and Kamber 2012). The titanite $^{207}\text{Pb}/^{235}\text{U}$ ratios exported from Iolite were identical irrespective of the $^{238}\text{U}/^{235}\text{U}$ used to calculate them, demonstrating that the degree of variation in $^{238}\text{U}/^{235}\text{U}$ shown by titanite (Hiess et al. 2012) would have no influence on our calculated U–Pb ages.

Both rutile and titanite U–Pb data were collected using dwell times that ultimately proved too short for the low count rates obtained with the analysed samples (Table S5). As a result of the short dwell times, a significant number of sweeps had zero counts on ^{206}Pb or ^{207}Pb for low-Pb grains. Once background-corrected, these zero counts became small negative numbers that resulted in extremely large negative spikes in the calculated $^{207}\text{Pb}/^{206}\text{Pb}$ ratio. Although Iolite provides an outlier rejection function designed to remove spikes from data, this did not appropriately correct for these large negative spikes, presumably due to their large magnitude and number. Consequently, a significant bias affected $^{207}\text{Pb}/^{206}\text{Pb}$ ratios, as identified by sometimes dramatic discrepancies between both the values and uncertainties of the measured $^{207}\text{Pb}/^{206}\text{Pb}$ versus the $^{207}\text{Pb}/^{206}\text{Pb}$ calculated from the measured $^{206}\text{Pb}/^{238}\text{U}$ and $^{207}\text{Pb}/^{235}\text{U}$ (assuming a $^{235}\text{U}/^{238}\text{U}$ of 137.818). We therefore employed an R script written for this purpose by T. Raupach, which modified the comma-delimited data files by averaging the measured intensities of every five integrations together (i.e. averaging sweeps 1–5, 6–10... etc.), thus simulating using a five-times-longer dwell time more appropriate to geochronology of our samples (Table S5). The R script produced new comma-delimited data files for each analysis with the calculated five-integration-averaged intensities, which were imported into Iolite and processed as usual. All data presented here were processed in this way. Using the longer simulated dwell times, the problem of negative spikes related to zero counts was eliminated for all titanites and almost all rutiles analysed, and no bias was observed between measured and calculated values for $^{207}\text{Pb}/^{206}\text{Pb}$ ratios and their uncertainties.

4.3.1 Rutile

Rutile U–Pb ratios were measured in a single analytical session, and employed a 50 μm spot size, repetition rate of 5 Hz, and an energy density on the sample of $\sim 2.9 \text{ J}/\text{cm}^2$. Six masses were measured in peak hopping mode: ^{206}Pb , ^{207}Pb , ^{208}Pb , ^{232}Th , ^{235}U , and ^{238}U . The 2845 Ma natural

rutile standard Wodgina (Ewing 2011) was used as a primary standard, relative to a $^{206}\text{Pb}/^{238}\text{U}$ of 0.555771 (the average of the four TIMS analyses presented by Ewing 2011). No common Pb correction was applied to primary standard Wodgina, as it was found to yield identical results corrected and uncorrected for common Pb. The 1095 Ma R10 rutile (Luvizotto et al. 2009) was analysed as a secondary standard. Dates ^{207}Pb -corrected for common Pb were calculated with Isoplot 3.7 (Ludwig 2012) using the Stacey and Kramers (1975) model common Pb composition for 1090 Ma for R10 and 60 Ma for sample rutiles. For the R10 standard, ^{208}Pb -corrected dates were also calculated in Iolite using the $^{208}\text{Pb}_{(\text{noTh})}$ correction provided by the VizualAge_UcomPbine data reduction scheme (Chew et al. 2014).

The R10 secondary standard was analysed regularly throughout the session to monitor accuracy. A weighted mean $^{206}\text{Pb}/^{238}\text{U}$ age of 1122 ± 9 Ma (95% confidence, MSWD = 0.7) was obtained for R10 uncorrected for common Pb, with an indistinguishable age of 1122 ± 9 Ma when ^{208}Pb -corrected for common Pb (Fig. S3a, b). This uncertainty does not include systematic uncertainties such as the long-term excess variance of $^{206}\text{Pb}/^{238}\text{U}$ dates of reference materials in our laboratory (Horstwood et al. 2016). We do not yet have a database to assess the long-term reproducibility of rutile geochronology in our laboratory, but taking a typical value of 2% for long-term excess variance (Horstwood et al. 2016) and propagating this uncertainty, the $^{206}\text{Pb}/^{238}\text{U}$ age of R10 would become 1122 ± 24 Ma. This age is within error of the concordia intercept age of 1095.2 ± 4.7 Ma for TIMS analyses of the R10 rutile (Luvizotto et al. 2009), confirming the accuracy of our rutile ages.

4.3.2 Titanite

Titanite U–Pb analyses were measured in two analytical sessions on a single day. They employed a 35 μm spot size, repetition rate of 5 Hz, and an energy density on the sample of ~ 2.9 J/cm². Eight masses were measured in peak-hopping mode: ^{201}Hg , ^{204}Pb , ^{206}Pb , ^{207}Pb , ^{208}Pb , ^{232}Th , ^{235}U , and ^{238}U .

The natural titanite standard MKED1 (1517.32 ± 0.32 Ma; Spandler et al. 2016) was used as a primary standard, and OLT1 titanite (1014.8 ± 2.0 Ma; Kennedy et al. 2010) as a secondary standard. A ^{207}Pb correction for common Pb was applied to primary standard MKED1. The radiogenic (i.e. common Pb corrected) isotope ratios from Spandler et al. (2016) were therefore used as reference values (following Horstwood et al. 2016). MKED1 has very low levels of common Pb compared to other titanite standards (Spandler et al. 2016).

A ^{207}Pb correction for common Pb was also applied to unknowns and secondary standard OLT1. Common Pb correction was performed using a model common Pb composition (Stacey and Kramers 1975), for an age of 1518 Ma for MKED-1, 1015 Ma for OLT1 and 60 Ma for titanite unknowns. ^{207}Pb -corrected ages were calculated from ratios using Isoplot 3.7 (Ludwig 2012).

The OLT-1 titanite standard was analysed regularly throughout both analytical sessions to monitor the accuracy of measurements. OLT1 analyses gave reproducible dates, with a weighted mean ^{207}Pb -corrected age of 1023 ± 7 Ma for eight analyses pooled from both analytical sessions (Fig. S3c, d). This age is within error of the reference age of 1015 ± 2 Ma (Kennedy et al. 2010), confirming the accuracy of our titanite U–Pb age determinations.

5 Results

5.1 Petrology of the breccia and blackwall units

We selected three samples from a ~ 73 m long drill core across the Margna–Malenco contact at Pass d’Ur. The drill cores were made available by the *Büro für Technische Geologie*, Chur. The 73 m long drill-core sampled 8.4 m of gneiss from the Margna nappe (quartz, plagioclase and amphibole), 24.8 m of brecciated material, ~ 30 m of micaschist, two layers of blackwall rocks of 1–2 m each, and ~ 11 m of serpentinized peridotite from the Malenco unit (Fig. 2a).

5.1.1 Brecciated material

The breccia is a mixture of both basement and ultramafic rocks, resulting in amphibole-rich clasts and chlorite-bearing gneiss clasts, made of quartz, plagioclase, amphibole, phlogopite and clinopyroxene. The breccia from Pass d’Ur displays a variable petrography from the contact with the crustal material towards the mantle rocks (Fig. 1).

The breccia can be subdivided into two units:

- Breccia A containing amphibole-rich clasts in a highly sheared phlogopite-white mica matrix (from 8.4 to 22.7 m depth; Fig. 2b);
- Breccia B made of chlorite-bearing gneiss clasts in a foliated chlorite–white mica matrix (from 22.7 to 33.2 m-depth; Fig. 2c).

There is no systematic variation of clast size and mineral proportions throughout the breccia. In breccia A, amphibole-rich clasts are rounded and elongated in the main foliation (Fig. 2b) and are decimetric to millimetric in size. Amphibole from amphibole-rich clasts are tremolite fibers (100–300 μm). At the thin-section scale, the tremolite-rich

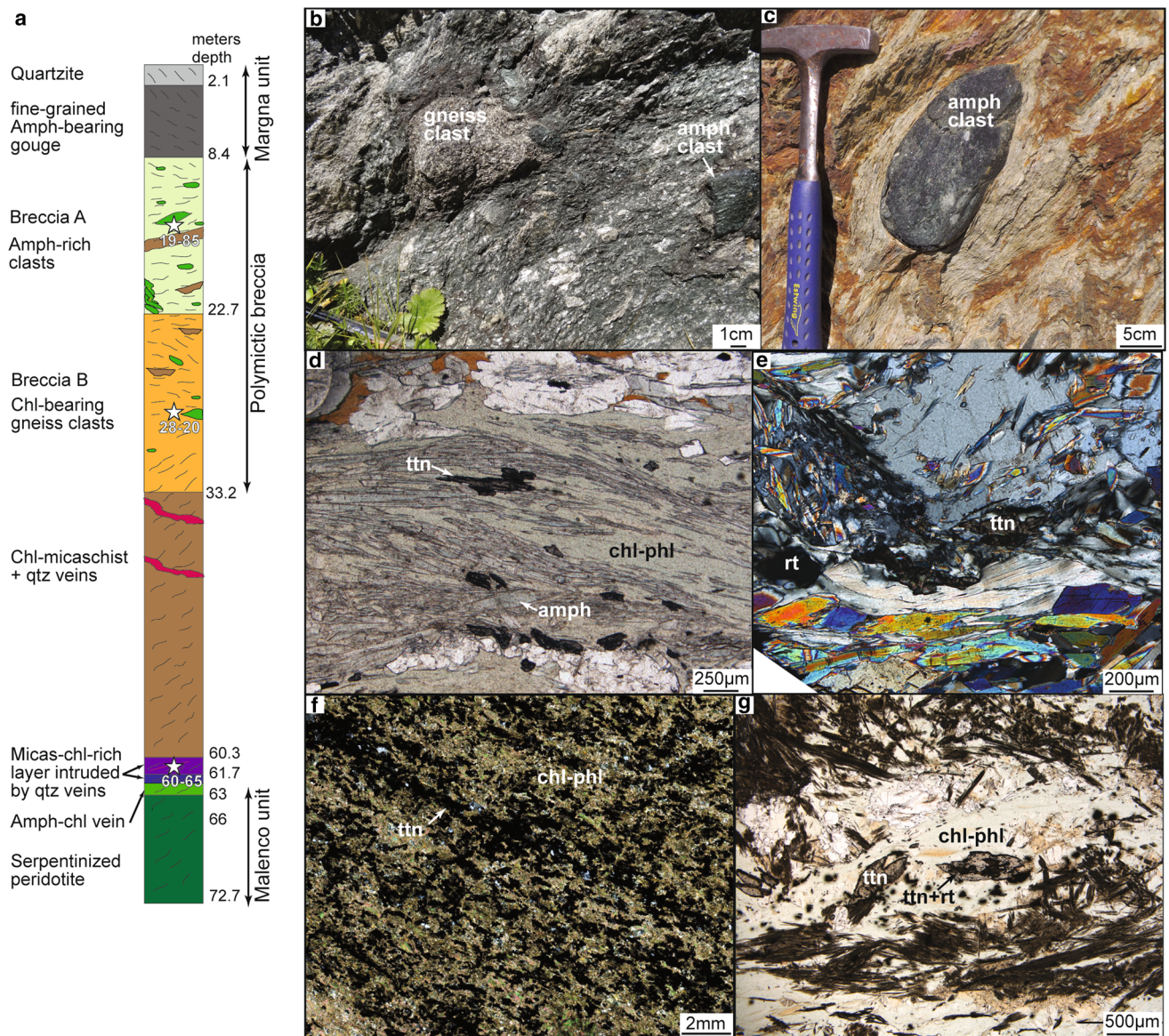


Fig. 2 **a** Log of the drill-core through the Margna crust, brecciated material, and serpentized peridotites from Malenco unit. White stars indicate location of the three studied samples; sample names are given as white text. **b** Field aspect of a gneissic and amphibole-rich clast in a chl-amph-mica rich matrix. **c** Field aspect of an amphibole-rich clast in a qtz-fsp-chl matrix. **d** Thin-section of Breccia A at 17.27 m depth in the core. Chlorite-phlogopite and amphibole-rich mm-thick shear zone separating feldspar porphyroblasts. Titanites surround

rutile grains. **e** Thin-section of Breccia A at 19.03 m depth in the core. Feldspar porphyroblasts surrounded by a chlorite and phlogopite shear zone containing titanite. **f** Thin section of the blackwall rocks at 60.64 m-depth in the core. Titanite idiomorphic grains are aligned in a chlorite-phlogopite matrix. **g** Thin section at 61.62 m depth in the core, also in the blackwall zone. Zoom on an idiomorphic titanite grain that overgrown rutile

clasts show little deformation of the tremolitic fibers. The matrix is greenish at the outcrop scale (chlorite-rich; Fig. 2b), made of chlorite + amphibole ± phlogopite + white mica, with accessory zircon, rutile and titanite. Tremolite and chlorite fibers are intergrown, forming highly sheared zones, intercalated with layers rich in quartz-feldspar porphyroblasts (Fig. 2d).

In breccia B, the size of the gneiss clasts varies from millimeter to meter-wide blocks (Fig. 2b). The matrix is

alternating between quartz-feldspar-rich and chlorite ± phlogopite rich layers, with accessory zircon, rutile and titanite grains (Fig. 2e).

5.1.2 Blackwall rocks

The rocks in contact with the micaschist unit below the brecciated material and the serpentized peridotites of the Malenco nappe are subdivided into: (1) a chlorite-rich

schist crosscut by quartz veins (Fig. 2f); and (2) a chlorite-amphibole-rich schist. The chlorite-rich schist is 1.4 m-thick and contains chlorite + biotite-phlogopite, zircon, rutile, titanite and apatite (Fig. 2f). Chlorite forms a foliation (main average foliation of N250/55 measured in the field) comparable to the surrounding micaschist unit. The chlorite-amphibole-rich schist is in contact with serpentinized mantle. This layer is black all along the serpentinized peridotite surface, and contains zircon and apatite but no titanite.

5.1.3 Analysed samples

We analysed rutile and titanite from three samples from the drill core (Figs. 2a, 3), two from the brecciated units and one from the blackwall zone. The first sample is from breccia A and contains a majority of amphibole-rich clasts at 19.85 m-depth (sample 19–85) whereas the second sample (sample 28–20) comes from the breccia B containing chlorite-bearing gneiss clasts at 28.20 m-depth. The third sample was taken from the chlorite-amphibole blackwall reaction zone of the core, at 60.65 m-depth (sample 60–65; Fig. 2).

5.2 Rutile–titanite occurrence

5.2.1 Brecciated material

In the breccia A, amphibole contains undeformed rutile grains ($< 10 \mu\text{m}$ in size; Fig. 2d), while bigger rutile (up to $100 \mu\text{m}$ in size) is included in feldspar porphyroblasts. Where feldspar porphyroblasts are fractured, the rutile is surrounded by titanite, but in undeformed porphyroblasts, rutile is shielded from titanite overgrowth. In the matrix, both titanite rimming rutile and titanite with no rutile cores are found. Titanite grains are elongated parallel to shear direction indicating syn-deformational growth (Fig. 2d).

In breccia B, amphibole and feldspar porphyroblasts contain rutile grains preserved from titanite overgrowth, and no pure titanite grains. Both titanite overgrowing rutile and pure titanite grains are found in the matrix, aligned in the foliation. In both breccias, slight zoning of titanite grains is visible with Backscattered Electron (BSE) images (Fig. S1).

5.2.2 Blackwall rocks

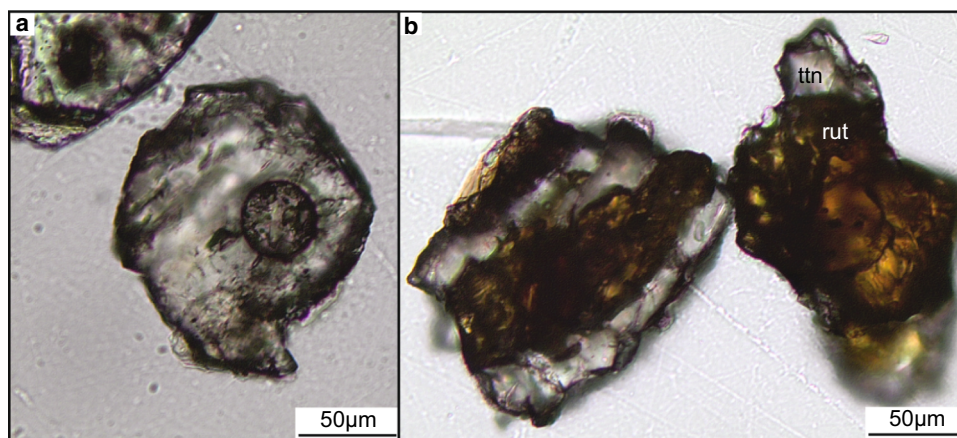
Chlorite-rich schists of the blackwall contain titanite with and without rutile cores in the chlorite–phlogopite matrix. Titanite grains are aligned in the main foliation and accumulated between domains that show different levels of deformation, ranging from highly sheared to undeformed (Fig. 2f). Titanite is euhedral, either with diamond or pentagonal shape. In this sample, titanite grains without rutile cores are mostly the smallest observed in the entire cored section ($50 \mu\text{m}$; Fig. 2h). Titanites that rim rutile grains are bigger, up to $500 \mu\text{m}$ (Fig. 2g). No zoning of titanite is visible with BSE images (Fig. S1).

5.3 Geochemistry of rutile and titanite

Major and trace element chemistry of rutile and titanite are reported in online Tables S1 and S2. Rutiles from sample 19–85 have 2.5–11.5 ppm U and 0.03–0.63 ppm Th, with an average of 6.4 ppm U. Rutiles from sample 28–20 have 0.3–12.2 ppm U and 0–0.22 ppm Th, with an average of 3.7 ppm U. Rutiles from sample 60–65 have 3.7–5.8 ppm U and 0.01–0.19 ppm Th, with an average of 4.7 ppm U. Measured concentrations of ^{206}Pb in rutiles (which includes both radiogenic and common Pb) were 0.03–0.21 ppm for 19–85, 0.003–0.23 ppm for 28–20, and 0.05–0.15 ppm for 60–65, with average ^{206}Pb concentrations of 0.11, 0.06 and 0.08 ppm respectively.

The trace elements measured in titanite grains from the three studied samples show convex LREE pattern and flat

Fig. 3 Titanite grains in an epoxy mount imaged in transmitted light on a petrographic microscope. **a** Analysed titanite from sample 60–65 and **b** titanite surrounding rutile from sample 19–85



HREE (Fig. S2). LREE concentrations are similar for the 3 samples; the HREE display a larger range for sample 28–20 and 19–85 (brecciated samples) than for sample 60–65 (blackwall zone; Fig. S2). Titanite from sample 19–85 has 4–27 ppm U and 2–5 ppm Th, with an average of 10 ppm U and 3 ppm Th. Titanite from 28–20 has 5–40 ppm U and 2–16 ppm Th, with an average 20 ppm U and 7 ppm Th. Titanite from 60–65 has 23–58 ppm U and 3–13 ppm Th, with averages of 43 ppm U and 9 ppm Th. Measured concentrations of ^{206}Pb in titanite (which includes both radiogenic and common Pb) were 0.2–1.9 ppm for 19–85, 0.2–1.9 ppm for 28–20, and 1.5–3.0 ppm for 60–65, with average ^{206}Pb concentrations of 0.5, 0.7 and 2.2 ppm respectively.

5.4 Geochronology

5.4.1 Use of the Wetherill concordia to calculate two-dimensional isochron ages

Rutile and titanites from the analysed samples have low U contents, which in combination with their young ages results in very low levels of radiogenic Pb (Pb^*). Consequently, the analysed rutiles and titanites have high to very high proportions of common Pb (Pb_c) relative to radiogenic Pb (Figs. 5, 6). Either a large common Pb correction must be applied to each analysis, or a two-dimensional isochron (so-called “SemiTotal-Pb/U isochron”) can be used to calculate a single age for each sample by applying a regression through data uncorrected for common Pb (Tera and Wasserburg 1972; Ludwig 1998, 2012). This rests on the assumption there are no inter- or intra-grain variations in age within samples, but this assumption can be tested by the fit of the data to the isochron. Both rutile and, in particular, titanite from each sample show a large range in the proportion of common Pb (Figs. 5, 6), making the resulting regression very well constrained. These samples are therefore ideally suited to the calculation of isochron ages. This method has the additional advantage of avoiding the need to assume a common Pb composition, which can instead be inferred directly from the data. We used a two-dimensional rather than three-dimensional isochron because of the large isobaric interference of Hg on ^{204}Pb that is unavoidable with LA-ICPMS (Horn et al. 2000; Andersen 2002; Gerdes and Zeh 2006), precluding accurate measurement of $^{204}\text{Pb}/^{206}\text{Pb}$ on our system.

We calculated rutile and titanite sample ages from two-dimensional isochrons on both Wetherill and Tera-Wasserburg concordia diagrams (Figs. 5, 6). In the literature, 2D isochron ages are typically calculated using a Tera-Wasserburg concordia diagram (e.g. Ludwig 1998; Storey et al. 2006; Warren et al. 2012; Chew et al. 2014). The young, low U titanites and rutiles analysed in this

study had extremely low Pb contents, resulting in the $^{207}\text{Pb}/^{206}\text{Pb}$ usually having lower precision than the $^{207}\text{Pb}/^{235}\text{Pb}$, with 2σ uncertainties on $^{207}\text{Pb}/^{206}\text{Pb}$ up to 1.8 times higher for both titanite and rutile analyses. The generally better precision on $^{207}\text{Pb}/^{235}\text{Pb}$ than $^{207}\text{Pb}/^{206}\text{Pb}$ motivates the use of a Wetherill concordia to perform the regression used to calculate 2D isochron ages for our samples, to allow the use of the most precise input data possible. Although Tera-Wasserburg concordias offer some advantages for visualisation of data and its concordance, Tera-Wasserburg and Wetherill concordia diagrams are mathematically equivalent and isochrons can be calculated on either type of concordia (Ludwig 1998, 2012). Thus, although it is intuitively easier to understand the use of the 2D isochron on the Tera-Wasserburg concordia, it is equally valid to perform these regressions on a Wetherill concordia (e.g. Ludwig 2012).

One reason the Tera-Wasserburg concordia is traditionally preferred for the calculation of isochron ages is that the isotopic composition of the common Pb component can easily be read off the concordia diagram: the intercept of the isochron with the y-axis corresponds to the $^{207}\text{Pb}/^{206}\text{Pb}_{\text{common}}$ (e.g. Ludwig 1998; Storey et al. 2006). Although it may be intuitively easier to understand on a Tera-Wasserburg concordia, exactly the same information about the isotopic composition of common Pb can be obtained from isochrons constructed on a Wetherill concordia: the $^{207}\text{Pb}/^{206}\text{Pb}_{\text{common}}$ can be calculated directly from the slope of the isochron, as we will illustrate below. To demonstrate this, in the following explanation we will describe the characteristics of an isochron defined by analyses that belong to a single age population but have differing proportions of common Pb. In this case, on a Wetherill concordia—as on a Tera-Wasserburg—the lower intercept of the regression with the concordia defines a concordant age with zero common Pb, and thus gives the common Pb-corrected age (Fig. 4a, b). On a Tera-Wasserburg diagram, the intercept of the regression with the $^{207}\text{Pb}/^{206}\text{Pb}$ axis (i.e. y axis) defines the common Pb composition. In the case of the Wetherill concordia diagram, the regression projects towards infinity and the common Pb composition cannot be read off an intercept. However, the slope of the isochron is given by

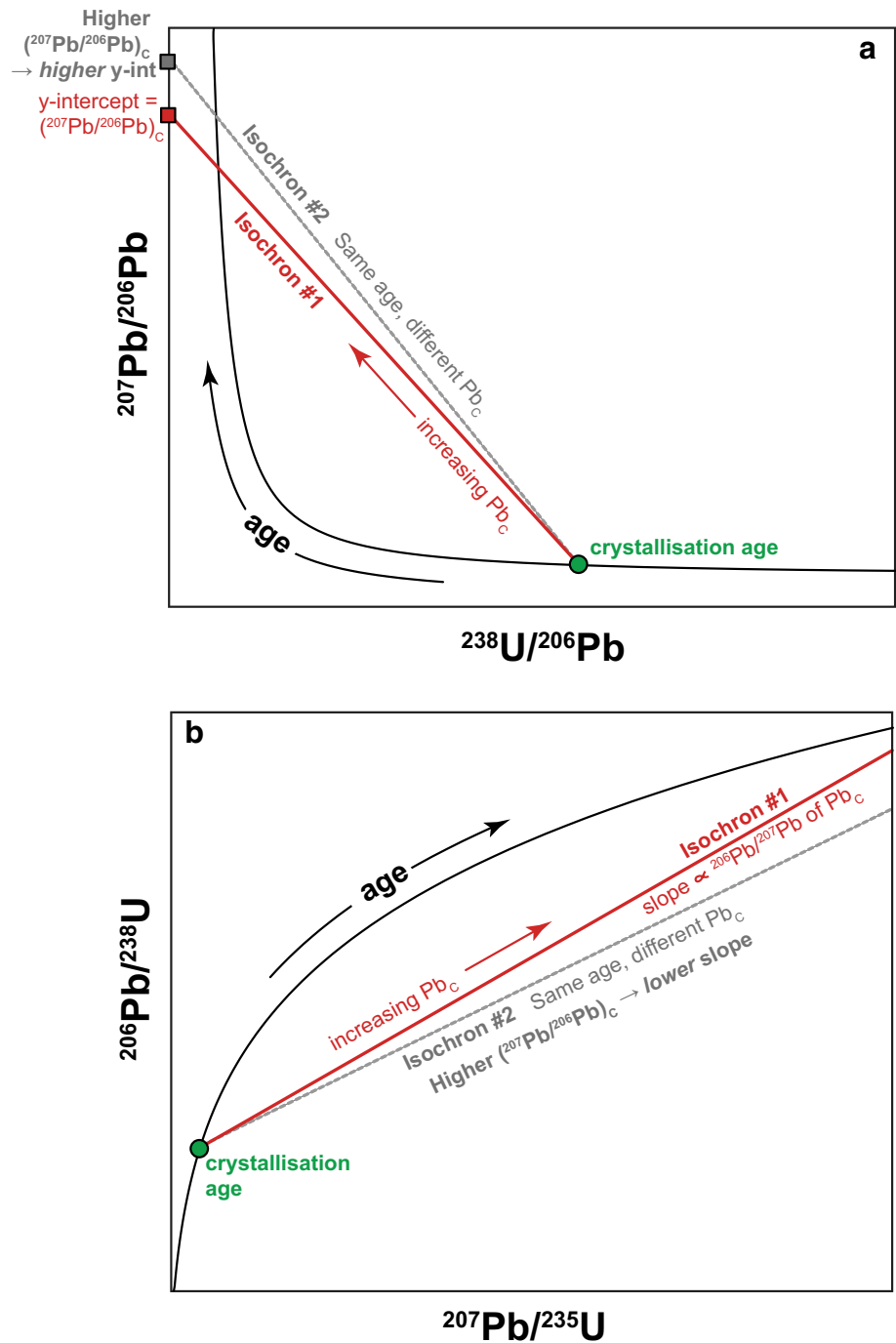
$$^{206}\text{Pb}/^{238}\text{U} \div ^{207}\text{Pb}/^{235}\text{U} \quad (1)$$

which is equivalent to

$$^{206}\text{Pb}/^{207}\text{Pb} \times ^{235}\text{U}/^{238}\text{U} \quad (2)$$

Since the $^{238}\text{U}/^{235}\text{U}$ is, at the scale we are interested in, essentially constant (at 137.818 ± 0.050 , taking the zircon value of Hiess et al. 2012), the $^{235}\text{U}/^{238}\text{U}$ equates to the

Fig. 4 Schematic illustration of the effect of different common Pb compositions on the isochron defined by data uncorrected for common Pb on a **a** Tera-Wasserburg and **b** Wetherill concordia diagram. Isochrons through a hypothetical array of data with the same age but a range of Pb^*/Pb_C are shown. For each plot, two isochrons with the same crystallization age but different common Pb compositions are shown. **a** On the Tera-Wasserburg concordia, the common Pb composition is given by the y-intercept of the isochron, while **b** on the Wetherill, it is the slope of the isochron that relates to the common Pb composition. See text for discussion



inverse of this value ($1/137.818$), allowing us to describe the slope as

$$^{206}Pb/^{207}Pb \times 0.007 \quad (3)$$

i.e. the slope is the $^{206}Pb/^{207}Pb$ multiplied by a constant. The $^{206}Pb/^{207}Pb$ represents the common lead composition (akin to the $^{207}Pb/^{206}Pb$ on the Tera-Wasserburg). Analyses with the same age but different proportions of common Pb will plot on a single regression, with the lower intercept of this isochron defined by the age and its slope defined by the

common Pb composition. With increasing proportions of common Pb, analyses will plot further away from the concordia in a 'northeasterly' direction, as both $^{207}Pb/^{235}Pb$ and $^{206}Pb/^{238}U$ increase with the addition of common Pb (which adds Pb but no U). Higher $^{207}Pb/^{206}Pb_{common}$ will give an isochron with a lower slope, and vice versa (Fig. 4b).

The isotopic composition of the common Pb is calculated from the slope of the isochron as follows:

$$^{207}Pb/^{206}Pb_{common} = \text{slope}_{isochron} \times 137.818 \quad (4)$$

We argue that the Wetherill concordia is a valuable alternative to the Tera-Wasserburg to calculate isochron ages and common Pb composition for young, low-U, and high Pb_C/Pb^* minerals. As we have shown above, it can provide the same information but allows use of the most precise input ratios available. The isotopic composition of common Pb is less immediately evident from visual inspection of the plot, but can easily be calculated from the slope. We advocate this calculation as an important step in interpreting Wetherill isochron ages, to ensure that the common Pb composition determined from the data is reasonable.

An alternative approach that would also allow the calculation of isochron ages from the more precise $^{206}Pb/^{238}U$ and $^{207}Pb/^{235}U$ ratios, while retaining the visualisation advantages of the Tera-Wasserburg diagram, would be to mathematically convert these ratios to the $^{238}U/^{206}Pb$ and $^{207}Pb/^{206}Pb$ ratios using an assumed $^{238}U/^{235}U$. This is facilitated by the fact that Isoplot (Ludwig 2012) offers the possibility to plot Tera-Wasserburg diagrams directly from the input ratios for a Wetherill concordia, by performing these mathematical conversions ‘behind the scenes’. However, the conversions performed by Isoplot are based on the assumption that the measured Pb was highly radiogenic ($^{206}Pb/^{204}Pb > 500$ –1000), and the Isoplot users’ manual stresses that when this assumption is invalid, the conversion provided by Isoplot must not be used (Ludwig 2012). The direct conversion of ratios in Isoplot is clearly invalid in the case of high-common-Pb minerals such as those dated in this study—noting that these are exactly the minerals that are well-suited to isochron ages. In such cases, Wetherill ratios can only be plotted correctly on a Tera-Wasserburg concordia by the geochronologist themselves converting ratios, and also calculating the ratio uncertainties and error correlations, following a series of exact equations (Ludwig 2012). This emphasizes the value of our approach, which directly calculates isochron ages on a Wetherill concordia using the ratios as measured, thus avoiding the need to manually mathematically convert ratios for plotting on a Tera-Wasserburg concordia. Below we present isochron ages for our rutile and titanite samples calculated on both Wetherill and Tera-Wasserburg concordia diagrams, and illustrate some cases in which use of the Wetherill concordia is advantageous—as well as some in which the Tera-Wasserburg is preferable.

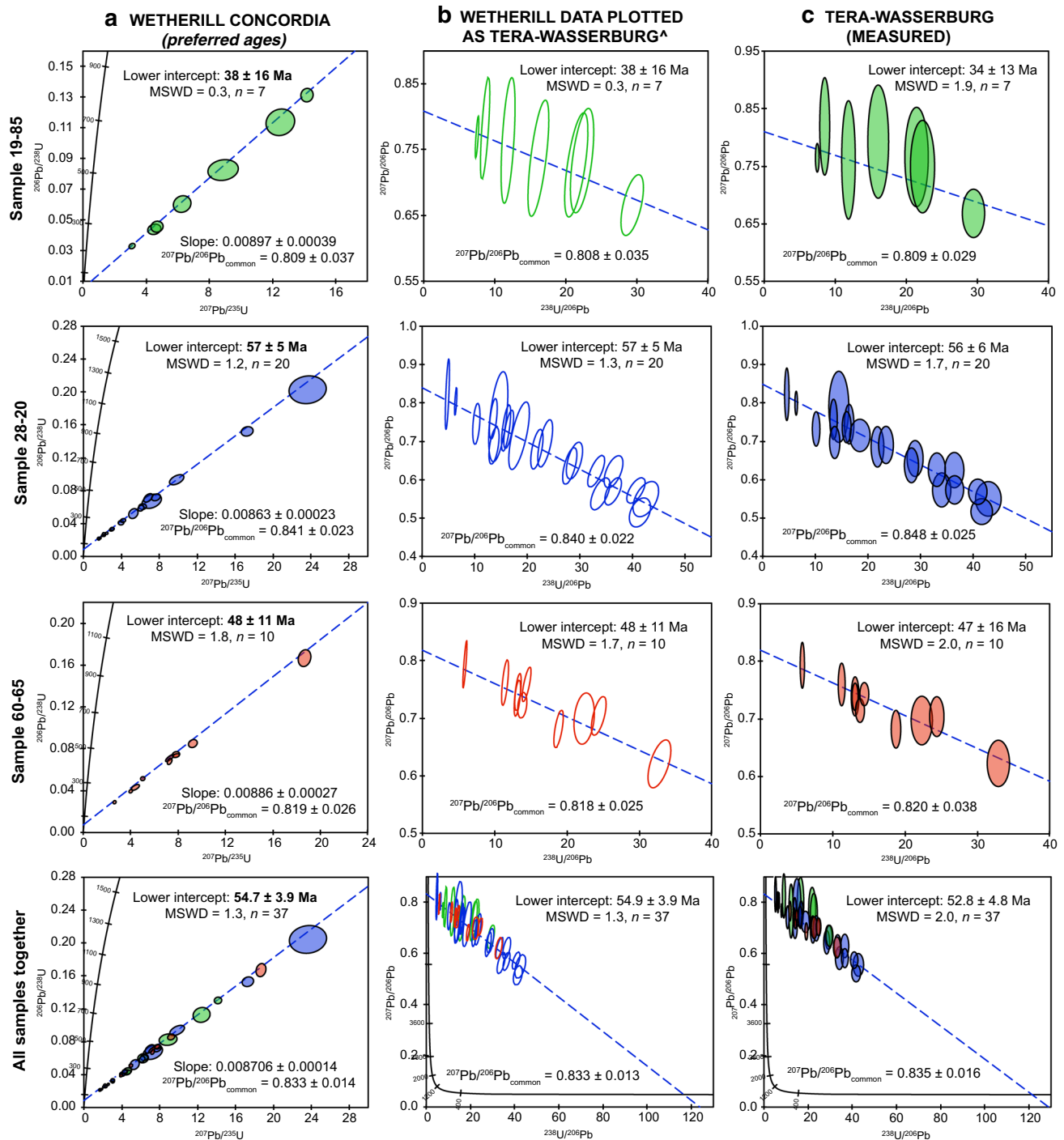
5.4.2 Titanite U–Pb geochronology

Isochron ages for titanites from the three samples were calculated in three ways: on Wetherill concordia, using the measured $^{206}Pb/^{238}U$ and $^{207}Pb/^{235}U$; on Tera-Wasserburg concordia using ratios calculated by Isoplot from the

Wetherill input ratios ($^{206}Pb/^{238}U$ and $^{207}Pb/^{235}U$); and on Tera-Wasserburg concordia directly using the measured $^{207}Pb/^{206}Pb$ and $^{238}U/^{206}Pb$ (Fig. 5). For the Wetherill concordia, the slope of the regression that defines the isochron, as well as its uncertainty, was output from Isoplot and used to calculate $^{207}Pb/^{206}Pb_{common}$ following Eq. 4 above (Fig. 5, Table 1). For both versions of the Tera-Wasserburg (calculated and measured), $^{207}Pb/^{206}Pb_{common}$ was determined from the y-intercept of the isochron, which was output with its uncertainty from Isoplot. Isochron ages were calculated for each of the three samples, and for all three samples together (Fig. 5).

For the same sample(s), isochron ages determined on the Wetherill and Tera-Wasserburg concordias are always within error. Except for sample 19–85, the Wetherill isochron age is always more precise than the Tera-Wasserburg isochron based on measured ratios (Fig. 5), demonstrating that the use of the most precise input ratios with the Wetherill concordia positively impacts the final precision on the isochron age. Wetherill and (measured) Tera-Wasserburg isochrons also give indistinguishable $^{207}Pb/^{206}Pb_{common}$ in each case. The Tera-Wasserburg concordia based on calculated ratios converted from the Wetherill input data plotted in Fig. 5 are not strictly correct, as the ratio and uncertainty conversion performed by Isoplot would only be valid for analyses with highly radiogenic Pb (Ludwig 2012; see Sect. 5.4.1). These Tera-Wasserburg concordia from calculated values are shown for comparison only, and demonstrate that directly calculating the isochron age and $^{207}Pb/^{206}Pb_{common}$ from the Wetherill concordia gives indistinguishable ages and common Pb compositions to converting the Wetherill ratios and plotting them on a Tera-Wasserburg diagram (Fig. 5). Our preferred U–Pb ages for the titanite samples are the Wetherill isochron ages, as they give the most precise sample ages and are also based on the most precise input ratios. We therefore restrict our following discussion to the Wetherill isochron ages.

For each of the three samples, individual analyses fit well to a single regression on a Wetherill concordia, as indicated by the low MSWDs of 0.3–1.8 (Fig. 5a), supporting a single age for all titanites from each sample. The isochrons for individual samples give imprecise lower intercept ages for samples 19–85 and 60–65, probably due mainly to the small number of analyses. Seven analyses of titanite from sample 19–85 gave a Wetherill isochron age of 38 ± 16 Ma with an MSWD of 0.3 (Fig. 5a). Twenty analyses of titanite from sample 28–20 gave a lower intercept of 57 ± 5 Ma, with an MSWD of 1.2 (Fig. 5a). Three analyses of titanite from sample 60–65 were excluded a priori and are not plotted or presented in data tables. One was excluded because in post-analysis inspection it was observed that the LA-ICPMS pit had drilled through



into a rutile core soon after the surface. The other two were excluded because they plotted extremely far from the isochron defined by other titanites from the same sample, with much older common Pb-corrected dates that are not reasonable for titanite in this sample. This is interpreted as the result of contamination by inclusions sampled during the drilling of the pit, and these analyses do not give meaningful dates. The remaining ten analyses of titanite from

sample 60–65 gave a lower intercept age of 48 ± 11 Ma, with an MSWD of 1.8 (Fig. 5a). The $^{207}\text{Pb}/^{206}\text{Pb}_{\text{common}}$ calculated from the Wetherill concordia isochron slope for each of the three samples were always indistinguishable within error (Fig. 5, Table 1). These isotopic compositions were also always within error of the Stacey–Kramers model common Pb composition for 60 Ma (0.839 ± 0.015 ; calculated in Squid 1.13).

◀**Fig. 5** Titanite U–Pb data for three samples individually (top three rows), and for pooled data from all three samples, distinguished by colour following the same scheme (bottom row). **a** Wetherill concordia plotting measured ratios. **b** Tera-Wasserburg concordia plotting ratios calculated from the $^{207}\text{Pb}/^{235}\text{U}$ and $^{206}\text{Pb}/^{238}\text{U}$, with the data conversion performed by Isoplot 3.7. ^aThese plots are shown for comparison only as the data conversion performed by Isoplot assumes that Pb is highly radiogenic (Ludwig 2012), which is incorrect for these samples. The data conversion is therefore not strictly correct. **c** Tera-Wasserburg concordia plotting the measured $^{207}\text{Pb}/^{206}\text{Pb}$ and $^{238}\text{U}/^{206}\text{Pb}$ ratios. Data on all types of concordia are plotted uncorrected for common Pb. Blue dashed lines are two-dimensional (semi-total Pb/U) isochrons calculated by Isoplot Ex 3.7. Lower intercept ages are given as text. Data are plotted at 2σ , and uncertainties on lower intercept ages are 95% confidence. The $^{207}\text{Pb}/^{206}\text{Pb}_{\text{common}}$ calculated from each isochron is given, calculated from the slope of the isochron following Eq. (4) for Wetherill concordia, and from the y-intercept of the isochron for Tera-Wasserburg concordia. Isochron slopes and y-intercepts, and their uncertainties, were determined by Isoplot 3.7. Note that for sample 19–85, with few analyses and a relatively small range in Pb_C/Pb^* , an anchored Tera-Wasserburg isochron may be more appropriate, and is given in online Fig. S4

Titanite from the three samples gave indistinguishable isochron ages, which are interpreted as dating crystallization of the titanite below the closure temperature of Pb (see Sect. 6.3), as well as indistinguishable common Pb compositions. In this case pooling of the dates from all samples is justified, to obtain a more precise age for the event in which the titanite formed. A 2D isochron age determined on a Wetherill concordia from all analyses pooled from the three samples ($n = 37$) gives an age of 54.7 ± 3.9 Ma, with an MSWD of 1.3 (Fig. 5a). The pooled isochron also gave the most precisely constrained common Pb composition, with $^{207}\text{Pb}/^{206}\text{Pb}_{\text{common}}$ of 0.833 ± 0.014 (Fig. 5a, Table 1). The nearly ideal MSWD indicates that all of the data fit well to the isochron, confirming the validity of pooling the data from the three samples. Our preferred age for the titanites from all three samples is this pooled isochron age of 54.7 ± 3.9 Ma, because it takes into account all of the data, and has the most precisely-constrained common Pb composition and age.

Table 1 Measured rutile and titanite U–Pb ages for the three studied samples from the Ur Breccia

Sample	Isochron age				Isochron type		Common Pb composition		
	Age (Ma)	\pm (95% conf.)	MSWD	n^a	Concordia type	Anchored isochron?	$^{207}\text{Pb}/^{206}\text{Pb}_{\text{common}}$	Source	Isochron slope ^b
Titanite ages									
19–85	38	16	0.3	7/7	Wetherill	Un-anchored	0.809 ± 0.037	Isochron slope	0.00897 ± 0.00039
28–20	57	5	1.2	20/20	Wetherill	Un-anchored	0.841 ± 0.023	Isochron slope	0.00863 ± 0.00023
60–65	48	11	1.8	10/10	Wetherill	Un-anchored	0.819 ± 0.026	Isochron slope	0.00886 ± 0.00027
Pooled (3 samples)	54.7	3.9	1.3	37/37	Wetherill	Un-anchored	0.833 ± 0.014	Isochron slope	0.008706 ± 0.00014
Rutile ages									
19–85	63.0	2.7	1.3	19/20 [26]	Tera-Wasserburg	Anchored	0.839 ± 0.015^c	Stacey–Kramers 60 Ma	
28–20	61	7	2.6	11/11 [23]	Tera-Wasserburg	Anchored	0.839 ± 0.015^c	Stacey–Kramers 60 Ma	
Pooled (2 samples)	62.4	3.3	1.9	30/31 [49]	Tera-Wasserburg	Anchored	0.839 ± 0.015^c	Stacey–Kramers 60 Ma	

^a n indicates the number of analyses included in the calculation of the age, as a fraction of the total number of analyses. For rutile, only analyses for which ^{207}Pb was distinguishable from background (> 50 cps) are included in this total; the total number of analyses including those with < 50 cps ^{207}Pb is given in square brackets

^bThe measured slope of isochrons is given for un-anchored Wetherill concordia only; for these isochrons the $^{207}\text{Pb}/^{206}\text{Pb}_{\text{common}}$ was calculated from the isochron slope as described in text

^cFor anchored Tera-Wasserburg isochrons, the quoted $^{207}\text{Pb}/^{206}\text{Pb}_{\text{common}}$ is an assumed model common Pb composition (Stacey and Kramers 1975), and is not inferred from the isochron itself

Common-Pb corrected dates were calculated for individual analyses using a ^{207}Pb correction and assuming a Stacey and Kramers (1975) model Pb composition for 60 Ma (Table S4). The extremely large magnitude of the common Pb correction for most of our analyses results in large uncertainties on individual ^{207}Pb -corrected dates, and makes them highly sensitive to the choice of common Pb composition. The individual ^{207}Pb -corrected dates are the equivalent of a 2D isochron age on a Tera-Wasserburg concordia, except that the $^{207}\text{Pb}/^{206}\text{Pb}$ is assumed rather than measured (Ludwig 1998), making comparison of the isochron ages and ^{207}Pb -corrected dates redundant. Since we regard isochron ages as the most robust method to correct for common Pb at such high proportions of $\text{Pb}_\text{C}/\text{Pb}^*$, we do not discuss ^{207}Pb -corrected dates here.

5.4.3 Rutile U–Pb geochronology

Rutile from samples 19–85 and 28–20 were analysed for U–Pb geochronology using a 50 μm spot (Table S3). We attempted to date rutile from sample 60–65, but the smaller grain size of rutile from this sample necessitated a 35 μm spot, and we could not obtain reliable U–Pb data for these young rutiles with this spot size. The lower count rates associated with the smaller spot were exacerbated by the absence of any higher-U grains in sample 60–65, which therefore could not be dated.

Rutile from samples 19–85 and 28–20 have variable and generally low U contents, which in combination with their young ages result in very low radiogenic Pb (Pb^*) contents. Nearly half of the rutile analyses had so little radiogenic Pb that the signal on radiogenic Pb isotopes (^{206}Pb and ^{207}Pb) was qualitatively indistinguishable from the background. Unsurprisingly, such data gave unreliable U–Pb ages, as evidenced by a much greater scatter in their U–Pb and Pb–Pb ratios. We therefore only considered data with > 50 counts per second (cps) on ^{207}Pb , to remove all analyses where Pb counts were effectively at background. This count rate is already background corrected. The threshold of 50 cps corresponds to raw count values (prior to background correction, and in counts not cps) of ~ 75 counts on ^{207}Pb . Background measurements had on average 18 counts on ^{207}Pb . The threshold of 50 cps on ^{207}Pb was chosen based on qualitative examination of the analytical spectra, in order to remove analyses that were visually indistinguishable, or nearly, from the spectra of background measurements. These analyses with < 50 cps ^{207}Pb are not shown in any data tables or plots. For the remaining analyses, outlier rejection using statistics relative to a median (rejection of 3 SD outliers relative to a median with MAD error) was employed in Iolite, instead of the mean with 3 SD outlier rejection used for titanite analyses. The median outlier rejection was found to work

better for low-Pb rutile analyses, which had noisy signals and occasional zero counts on ^{207}Pb or ^{206}Pb . Using a mean outlier rejection for rutile analyses sometimes resulted in a bias in $^{207}\text{Pb}/^{206}\text{Pb}$ ratios, and higher uncertainties, compared to the $^{207}\text{Pb}/^{206}\text{Pb}$ calculated from the measured $^{206}\text{Pb}/^{238}\text{U}$ and $^{207}\text{Pb}/^{235}\text{U}$.

Rutile U–Pb data for each sample and for pooled data from both samples define a single isochron on both a Wetherill and Tera-Wasserburg concordia (Fig. 6a, b). Like for titanites, unanchored isochron ages were indistinguishable whether calculated on a Wetherill (Fig. 6a) or Tera-Wasserburg concordia, and whether measured (Fig. 6b) or calculated (not shown) ratios were plotted on the Tera-Wasserburg, but Wetherill isochrons gave the most precise isochron ages in most cases (Fig. 6a, b). However, rutiles have less spread in $\text{Pb}_\text{C}/\text{Pb}^*$ than titanites, with much lower maximum values of $\text{Pb}_\text{C}/\text{Pb}^*$ (Fig. 6, cf Fig. 5). Consequently, the isotopic composition of common Pb is much less well constrained from the isochron defined by the data for the rutiles compared to the titanites. This is seen by the large uncertainties on the $^{207}\text{Pb}/^{206}\text{Pb}_\text{common}$ calculated from the isochron slopes or y-intercepts (Fig. 6), and contributes a significant uncertainty to the final age calculated from unanchored isochrons. The $^{207}\text{Pb}/^{206}\text{Pb}_\text{common}$ calculated from an unanchored isochron is always within error of the model Pb composition for 60 Ma of 0.839 ± 0.015 (Stacey and Kramers 1975; calculated by Squid 1.13), but is much less precisely constrained (Fig. 6). Ages were therefore also calculated from isochrons anchored to a $^{207}\text{Pb}/^{206}\text{Pb}_\text{common}$ of 0.839 ± 0.015 , resulting in indistinguishable ages but dramatically improved age precision (Fig. 6c). One major disadvantage of the Wetherill concordia in this context is that Isoplot does not allow an isochron to be anchored to a specific $^{207}\text{Pb}/^{206}\text{Pb}_\text{common}$ either for a Wetherill concordia, or for a Tera-Wasserburg concordia plotting data calculated from Wetherill ratios. Anchored isochron ages were therefore only calculated for measured Tera-Wasserburg ratios. Our preferred ages are these anchored Tera-Wasserburg isochron ages (Fig. 6c), and only these are discussed below.

Twenty-six rutiles from sample 19–85 were analysed, of which six gave < 50 cps ^{207}Pb and were discarded. Of the remaining twenty analyses, one had a pronounced zone of raised Pb with a significantly different $^{207}\text{Pb}/^{206}\text{Pb}$, probably as the result of sampling an inclusion, and was excluded. The remaining nineteen analyses contain variable, but always non-zero, proportions of common Pb. They gave an anchored Tera-Wasserburg isochron age of 63.0 ± 2.7 Ma that we interpret as the sample rutile age. The good MSWD of 1.3 for this regression indicates that all analysed rutiles fit well to the isochron and belong to a single age population.

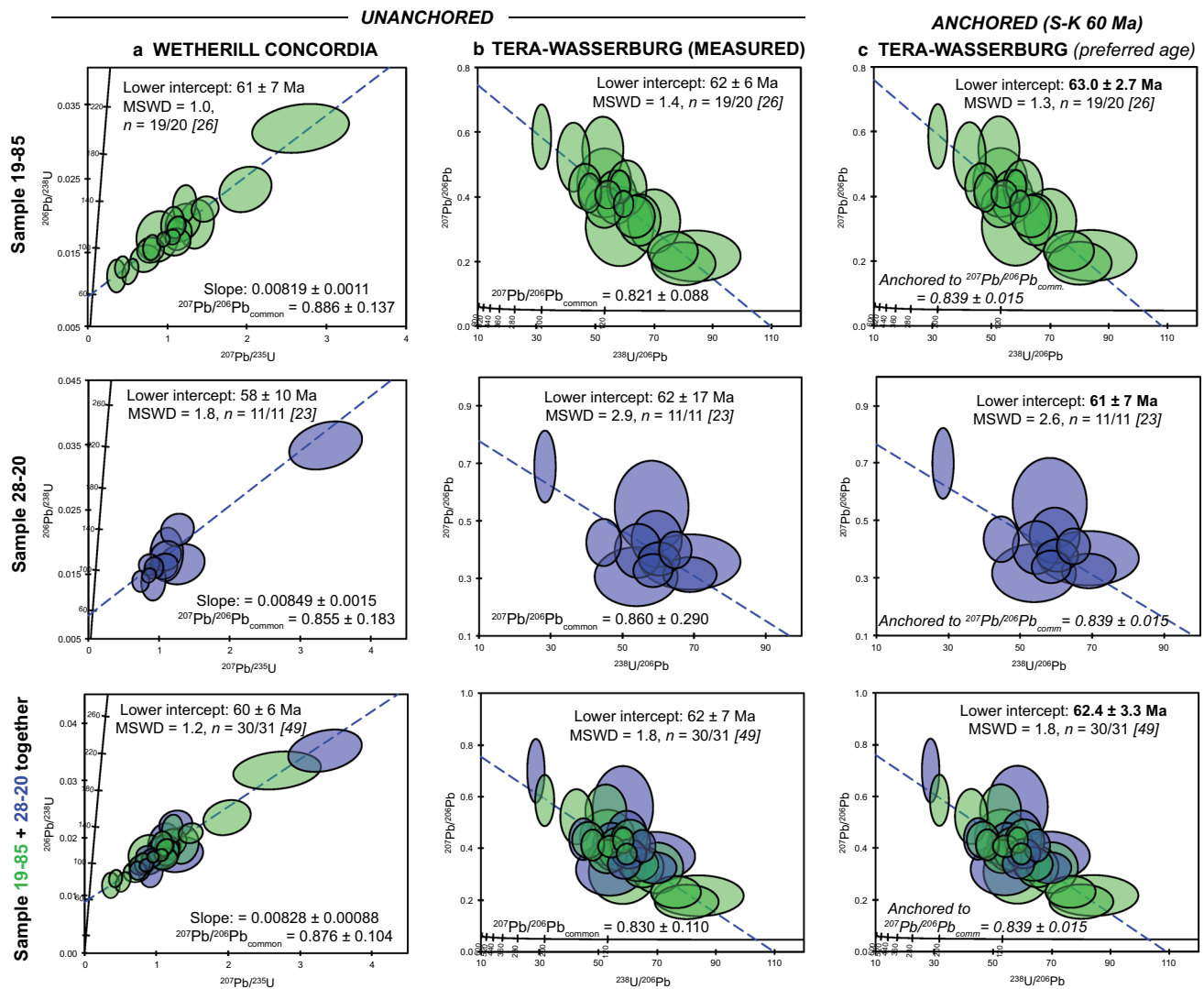


Fig. 6 U–Pb data for rutile from two samples and for both samples together, plotted uncorrected for common Pb on concordia diagrams. Only analyses with ≥ 50 cps ^{207}Pb are plotted; below this, Pb signals were not significantly above background and so did not yield reliable U–Pb ratios. n indicates the number of analyses considered as a fraction of the total number of analyses with ≥ 50 cps ^{207}Pb ; the total number of analyses including those with < 50 cps ^{207}Pb is given in square brackets. **a** Wetherill concordia and **b** Tera-Wasserburg

Twenty-three rutiles from sample 28–20 were analysed, of which twelve gave < 50 cps ^{207}Pb and were discarded, leaving only eleven acceptable analyses. The U content of rutile from this sample is on average lower than for 19–85 (Sect. 4.3), resulting in few grains with measurable Pb that can be used to constrain an age for this sample precisely. Nonetheless, the eleven analyses define an anchored Tera-Wasserburg isochron with a lower intercept age of 61 ± 7 Ma and an MSWD of 2.6 (Fig. 6c). Furthermore, when the eleven useable 28–20 rutile analyses are plotted together with the data from 19–85 rutiles, it can be seen that rutiles from the two samples have indistinguishable

concordia plotting ratios as measured, both with an unanchored isochron plotted by Isoplot 3.7; lower intercept age and common Pb composition calculated from these isochrons are given as text. **c** Tera-Wasserburg concordia plotting measured ratios and with an isochron anchored to the Stacey–Kramers model Pb composition for 60 Ma; lower intercept ages are given as text. Our preferred ages are the anchored Tera-Wasserburg isochron ages (**c**), which are the most precise

ages, at the relatively low precision achievable with in situ analysis. The combined data from 19–85 and 28–20 rutiles define a single anchored isochron on a Tera-Wasserburg concordia, as confirmed by a reasonable MSWD of 1.8. The lower intercept age of 62.4 ± 3.3 Ma is indistinguishable from that of 19–85 rutiles alone, indicating that rutiles from both samples record the same age. The preferred age for rutiles from both samples is the isochron age of 63.0 ± 2.7 Ma for sample 19–85, which is the most precise.

Individual $^{206}\text{Pb}/^{238}\text{U}$ dates were Pb_C-corrected using a ^{207}Pb correction (Table S3). As discussed in Sect. 5.4.2, it

is redundant to compare ^{207}Pb -corrected dates and isochron ages, and these are not discussed here. ^{208}Pb -corrected dates were not calculated for rutiles. Although rutile usually contains negligible Th, making it particularly well-suited to a ^{208}Pb -correction for common Pb (Zack et al. 2011), the majority of analysed rutiles in this study showed significant counts on ^{232}Th (see Table S3). The $^{208}\text{Pb}_{(\text{noTh})}$ correction offered by VizualAge_UcomPbine assumes that the concentration of Th, and thus thorogenic Pb, is zero, and will therefore overcorrect for common Pb if any Th is present.

5.4.4 Propagation of systematic uncertainties

The isochron ages do not take account of sources of systematic uncertainties, such as the long-term reproducibility of the technique and the uncertainties in the reference ratios of the primary standard, which must be propagated onto the sample age to allow comparison with ages from other geochronometers, labs or analytical sessions (Horstwood et al. 2016). We do not have a database to assess long-term excess variance of U–Pb geochronology of titanite or rutile in our laboratory, and instead took a typical value for U–Pb dating of 2% (Horstwood et al. 2016) as representative. Propagating this estimate of long-term reproducibility along with the uncertainties in the reference ratios (as determined by the 2 s.e. variability of the $^{206}\text{Pb}/^{238}\text{U}$ ratio of TIMS aliquots of Spandler et al. (2016) for MKED-1 titanite and Ewing (2011) for Wodgina rutile), the isochron ages including systematic uncertainties become 54.7 ± 4.1 Ma for titanite from the three samples and 63.0 ± 3.0 Ma for rutile from two samples.

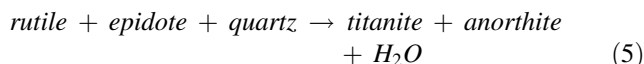
6 Discussion

6.1 Petrographic evidence for the timing of rutile and titanite growth

Textural evidence shows that rutile is either included in feldspar, or rimmed by titanite. In the brecciated units, the occurrence of titanite rims around rutile cores indicates that titanite formed at the expense of rutile. In the matrix, we observed both titanite grains, and titanite rims surrounding rutile cores. Titanite mainly grows in the main foliation made of feldspar, epidote, chlorite, actinolite and white mica, which relates to the Alpine orogeny, and is locally deformed by this foliation. The microtextural setting of titanite therefore indicates that it formed at the expense of rutile during Alpine metamorphism, in agreement with the observations of Sidler and Benning (1992). Rutile included in unaltered and undeformed feldspar is not replaced by

titanite, suggesting that rutile inclusions were shielded from the titanite-forming reaction.

Sidler and Benning (1992) proposed that the titanite-producing reaction in the Ur breccia was:



based on their observation of rutile and epidote as inclusions in feldspar porphyroblasts but almost nowhere else, with titanite in the matrix, and oligoclase rims on albite. This reaction, known as the TZARS reaction, has a moderate positive slope in P–T space (Frost et al. 2001; Kapp et al. 2009), such that formation of titanite at the expense of rutile could relate to either heating, decompression, or both. Frost et al. (2001) described this reaction as defining the high pressure limit for titanite in plagioclase bearing rocks, and point out that titanites rimming rutiles are commonly interpreted as a decompression texture. Kapp et al. (2009) also emphasized the pressure sensitivity of the TZARS reaction, and exploited it to propose its use as a geobarometer. The exact position of the reaction in P–T space is not well defined, and is dependant on bulk composition (notably Ca; Frost et al. 2001), and the activity of anorthite (a_{an}) and clinozoisite (a_{czo}) and therefore on Na and Fe^{3+} (Kapp et al. 2009). Based on the occurrence of titanite in natural samples, the transition should occur at > 6 kbar at 400°C (Frost et al. 2001). Although it is difficult to precisely relate titanite growth to a specific point in the Alpine metamorphic evolution, there is only one part of the established clockwise P–T path for the Malenco unit during the Alpine orogeny which corresponds to the appropriate conditions to form titanite at the expense of rutile by the reaction proposed by Sidler and Benning (1992) (i.e. heating or decompression from moderate P and T). These conditions correspond to the Alpine thermal maximum ($\sim 460^\circ\text{C}$, Benning and Sidler 1992). We cannot distinguish whether titanite formed during heating or subsequent decompression, but nonetheless titanite growth is bracketed to a reasonably restricted part of the Alpine metamorphic evolution. The timing of rutile formation is less well constrained by textural evidence, which indicates that rutile predates titanite, but does not constrain whether rutile formed during an earlier phase of the Alpine evolution or is a pre-Alpine relict mineral phase.

6.2 Rutile age interpretation

The well-constrained anchored Tera-Wasserburg isochron age of 63.0 ± 2.7 Ma for rutile from sample 19–85 is taken as the U–Pb age of rutile from both 19–85 and 28–20, given the good fit of the few analyses of 28–20 that contained measurable Pb to the same isochron as 19–85 rutiles and the indistinguishable isochron age of 62.4 ± 3.3 Ma

for pooled data from both samples (Sect. 5.4.3). The rutile U–Pb age of 63.0 ± 3.0 Ma (including systematic uncertainties) for these two samples could record either (1) cooling through the closure temperature of Pb in rutile, or (2) growth of rutile below its closure temperature. The closure temperature of Pb in rutile (T_C (Pb–Rut)), which depends on the grain size and cooling rate, is a matter of ongoing debate. The original empirical calibration of T_C of rutile (380–420 °C; Mezger et al. 1989) has been revised to 500–540 °C when modern values for the closure temperatures of the calibrating geochronometers are taken into account (Vry and Baker 2006). Diffusion experiments gave a higher T_C (Pb–Rut) for comparable grainsizes and cooling rates, comprised between 580 and 630 °C (Cherniak 2000). The higher T_C (Pb–Rut) has been corroborated by a second empirical field calibration (Vry and Baker 2006) and modelling of diffusion profiles of Pb in natural rutiles (Kooijman et al. 2010). Importantly, all studies give a T_C (Pb–Rut) of 500 °C or higher. Considering that Alpine metamorphism did not exceed 460 °C (Mellini et al. 1987; Benning and Sidler 1992), this implies that if rutile had grown before Alpine metamorphism, its U–Pb age would not have been affected by the Alpine overprint. Given that the rutile U–Pb isochron age of 63.0 ± 3.0 Ma is clearly an Alpine age, this in turn implies that rutile must have grown during the Alpine orogeny, and its age therefore dates rutile crystallization during Alpine metamorphism.

Textural relationships cannot link rutile growth to a specific part of the Alpine P–T evolution, but clearly demonstrate that rutile predates titanite. This suggests that rutile grew in the earlier part of the Alpine evolution, at relatively high pressures prior to the decompression event in which titanite formed. Although the exact P–T stability field of rutile is strongly dependent on bulk composition, experimental and empirical evidence for a wide range of compositions shows that rutile is the titanium phase stable at highest pressures (e.g. Bohlen et al. 1983; Bohlen and Liotta 1986; Liu et al. 1996; Ernst and Liu 1998; Frost et al. 2001; Zack and Kooijman 2017). Since peak pressures during the Alpine evolution did not exceed 0.7 GPa (Benning and Sidler 1992), rutile likely grew at or close to the Alpine pressure peak.

6.3 Titanite age interpretation

The three analysed samples were collected within 20 m in a single drill-core and gave indistinguishable titanite U–Pb ages. The excellent fit of all three samples to the pooled isochron, with a MSWD of 1.3 supports the interpretation that titanite in all three samples have the same age and allows us to take the combined lower intercept age of 54.7 ± 4.1 Ma (including systematic uncertainties) as the best estimate of the age of titanite from all samples.

The closure temperature (T_C) of Pb in titanite is now generally acknowledged to be in excess of 800 °C, based on several recent studies of natural samples from regions in which the thermal evolution is unusually robustly and precisely constrained (Kohn and Corrie 2011; Gao et al. 2012; Spencer et al. 2013; Stearns et al. 2016). A wide range in early estimates for the closure temperature (T_C) of Pb in titanite (e.g. 450–500 °C, Mattinson 1978, to $> 680 \pm 20$ °C, Scott and St-Onge 1995) at least partly reflects difficulties in relating titanite ages in a given rock to a specific temperature, given the ability of titanite to crystallise over a large temperature range (Kohn 2017). An experimental determination of the closure temperature (T_C) of Pb in titanite returned a moderate closure temperature of ~ 600 °C for 100 μ m grains at cooling rates of 10 °C/Ma (Cherniak 1993), but this was in conflict with much lower diffusivities determined for the similarly sized and charged Sr in titanite (Kohn 2017). Evidence is now overwhelmingly in favour of similar diffusivities for Sr and Pb in titanite and a $T_C > 800$ °C for Pb in titanite (Marsh and Smye 2017; Holder et al. 2019; Kohn 2017).

Given the evidence for growth of titanite from rutile during Alpine metamorphism (Sect. 5.1), and the fact that temperatures during Alpine metamorphism in the Val Malenco did not exceed 500 °C (Mellini et al. 1987; Benning and Sidler 1992), which is well below the T_C of Pb in titanite, the young (54.7 ± 4.1 Ma) age of titanite from the Ur samples must record growth of titanite below the T_C of Pb during the Alpine orogeny. This is consistent with the lack of age variations between and within titanite grains, in contrast to what might be expected if they were cooling ages produced by diffusive loss of Pb.

6.4 Zr concentration of rutile and titanite

The Zr concentrations of either rutile or titanite equilibrated with the appropriate buffering assemblage can be used as a so-called single mineral thermometer. The required buffering assemblage for Zr-in-rutile thermometry is quartz + zircon (Ferry and Watson 2007; Tomkins et al. 2007; Watson et al. 2006; Zack et al. 2004). For Zr-in-titanite thermometry, equilibrium with zircon + quartz + rutile is required (Hayden et al. 2008). The analysed rutiles and titanites are unlikely to have formed in equilibrium with the appropriate assemblages to perform Zr thermometry. Breccia A is dominantly mafic–ultramafic in composition and is poor in quartz; the chlorite-bearing gneiss clasts contain quartz and zircons that originated prior to brecciation. At the relatively low temperatures of formation of rutile and titanite, equilibrium between all of the phases in the buffering assemblage—even if present—is increasingly unlikely. This has been demonstrated by Cruz-Uribe et al. (2018), who showed that

titanites from a wide variety of samples that equilibrated at $< 600\text{ }^{\circ}\text{C}$ did not form in equilibrium with the buffering assemblage, even though the appropriate minerals were present in the rock. In these samples, Zr-in-titanite temperatures gave unreasonably high and scattered temperatures, leading Cruz-Urbe et al. (2018) to conclude that the single mineral thermometers cannot be assumed to be reliable at moderate–low temperatures. Our rutiles and titanites formed during Alpine metamorphism which likely did not exceed $460 \pm 30\text{ }^{\circ}\text{C}$ (Benning and Sidler 1992) so a lack of chemical equilibrium at the necessary scale is to be expected. It is therefore not meaningful to calculate Zr-in-rutile and Zr-in-titanite temperatures. This is supported by highly variable Zr contents, particularly for titanite, with concentrations for both minerals ubiquitously giving temperatures that are significantly higher than the thermal maximum determined for Alpine metamorphism in this region. We do not present temperatures calculated from Zr contents of rutile and titanite given that we regard these as meaningless. A very good constraint on the maximum temperature is given by the P–T conditions of breakdown of antigorite to forsterite plus talc. Experiments on serpentinite show that the maximum temperature that can be reached by the system before this breakdown occurs is $520\text{--}540\text{ }^{\circ}\text{C}$ at 5 kbar (Ulmer and Trommsdorff 1999), and olivine + tremolite are produced at $\sim 500\text{ }^{\circ}\text{C}$ at 5 kbar. As the serpentinites from Malenco did not undergo breakdown to olivine + talc, nor is there evidence for olivine + tremolite at the expense of antigorite + diopside, we infer that $500\text{ }^{\circ}\text{C}$ is the maximum temperature reached during regional metamorphism in the Malenco ultramafic rocks and the surrounding region.

6.5 Significance of rutile and titanite growth ages: comparison with previous geochronology

Our data show that rutile in the Pass d'Ur samples grew at $63.0 \pm 3.0\text{ Ma}$ during the higher pressure part of the Alpine metamorphic evolution. Our dated titanites from the same samples grew at $54.7 \pm 4.1\text{ Ma}$ either during the thermal maximum or the following decompression. The rutile age is just outside of error older than the titanite age, consistent with the textural observations that indicate that rutile predates titanite, which formed at its expense. The close ages for rutile and titanite imply a relatively short timespan between high pressure conditions and the subsequent decompression. Taking into account the relatively low precision of our ages for these low U minerals, the maximum time permissible between high pressure conditions and decompression, as recorded by rutile and titanite growth respectively, is $\sim 15\text{ Myr}$.

Our study area is located in the footwall of the Lunghin–Mortirolo movement zone (Fig. 1a), a regional-scale shear zone that separates weakly deformed rocks in the hangingwall from ductile Alpine deformation in the footwall (Mohn et al. 2011). We compiled ages for geochronometers with moderate closure temperatures measured on both sides of the Lunghin–Mortirolo movement zone from the literature (Hunziker et al. 1992; Bachmann et al. 2009; Handy et al. 1996; Villa et al. 2000; Price et al. 2018) and evaluated their significance with respect to the new rutile and titanite data (Fig. 1). The reviewed geochronometers have a range of closure temperatures for diffusional resetting: $\geq 550\text{ }^{\circ}\text{C}$ for Ar–Ar amphibole; $500\text{--}550\text{ }^{\circ}\text{C}$ for Rb–Sr in white mica; and $350\text{--}450\text{ }^{\circ}\text{C}$ for K–Ar/Ar–Ar in white mica and biotite (Siegesmund et al. 2008; Bachmann et al. 2009; Price et al. 2018, and refs therein). However, given the relatively low temperatures of Alpine overprinting in the eastern Central Alps, if re-equilibration of these geochronometers occurred during the Alpine orogeny it was mostly by recrystallisation rather than thermally-activated diffusion. This means that the resulting ages do not necessarily relate to their closure temperatures, and instead record recrystallisation. This has two implications: (1) the different geochronometers, including our titanite growth ages, may be expected to record similar ages in spite of their diverse closure temperatures, if the different minerals all completely recrystallised or grew in the same event; and (2) very different ages may be expected between samples according to whether or not recrystallisation occurred, for example due to different degrees of deformation and/or fluid ingress. Incomplete recrystallisation of pre-existing minerals would lead to a mixed age between the older (inherited) and newly recrystallised components.

Below the Lunghin–Mortirolo movement zone (i.e. in its footwall), the available data are K–Ar ages on phengites (Hunziker et al. 1992) from a few localities in the Margna nappe ranging from Pass d'Ur to Maloja (Fig. 1) and a few white mica Ar–Ar (Price et al. 2018) and Rb–Sr isochron ages (Bachmann et al. 2009). The phengite K–Ar ages vary from $69.3 \pm 3.2\text{ Ma}$ to $61.2 \pm 2.6\text{ Ma}$, broadly overlapping with our new rutile age, while muscovite K–Ar ages are more variable from 75 to 270 Ma (Hunziker et al. 1992), indicating incomplete overprinting during Alpine metamorphism.

Within the LMMZ, amphiboles from the Platta unit (Fig. 1) were dated by Ar–Ar and gave plateau ages of 69.4 ± 2.6 and $75.0 \pm 1.2\text{ Ma}$ (Handy et al. 1996), while white micas from Platta gave “integrated” (non-plateau) Ar–Ar ages of 61.9 ± 1.7 and $62.6 \pm 1.2\text{ Ma}$ (Price et al. 2018). Approximately 5 km to the northeast, still within the LMMZ, K–Ar ages on stilpnomelane and amphibole are 63.4 ± 1.0 and 59.4 ± 7.4 , respectively (Hunziker et al. 1992). South of the Engadine line in the area of Piz

Corvatsch (Fig. 1), still within the LMMZ, Rb–Sr isochrons between recrystallised white mica and calcite, feldspar or apatite gave ages of 53.85 ± 0.59 Ma and 47.1 ± 0.4 Ma for a quartz micaschist and calc-silicate from the Platta nappe, and 48.6 ± 0.7 Ma for a quartz mylonite from the basal Austroalpine units south of the Engadine line (Fig. 1) (Bachmann et al. 2009). White mica in these samples was recrystallised during Alpine deformation below the closure temperature for Rb–Sr, so these ages were interpreted to directly date Alpine deformation (Bachmann et al. 2009). Other samples dated by the Rb–Sr isochron technique had excessively high MSWDs (up to 2537), indicating isotopic disequilibrium between the analysed phases (Bachmann et al. 2009), and are not discussed here. A nearby sample from the Platta nappe gave an “integrated” white mica Ar–Ar age of 50 ± 0.6 Ma (Price et al. 2018). Although this sample did not give a true plateau age, it has one of the more coherent Ar–Ar spectra available, with large proportion of steps close to 50 Ma. This could be interpreted as recording more complete recrystallisation of white mica in this sample, which is close to the LMMZ, at c. 50 Ma. Collectively, all of the Ar–Ar and K–Ar ages from within the LMMZ broadly agree with both the well-equilibrated Rb–Sr ages of Bachmann et al. (2009) and our new titanite ages.

In contrast, all K–Ar and Ar–Ar ages on weakly deformed samples from the hangingwall of the LMMZ indicate ages exceeding 200 Ma for both muscovite and biotite (e.g. Hunziker et al. 1992; Price et al. 2018) suggesting that the thermal overprint during Alpine metamorphism was < 350 °C in the hangingwall of the LMMZ, consistent with the lower greenschist metamorphism recorded in the Bernina-Err units. This indicates that micas in the weakly deformed hangingwall of the LMMZ were not recrystallised, while below the LMMZ the much younger mica ages testify to partial or complete recrystallisation during Alpine deformation. Handy et al. (1996) obtained K–Ar ages, ranging from 67.5 ± 2.0 Ma to 89.1 ± 2.7 Ma, for a series of white micas from Mesozoic sediments from the lower Austroalpine Err nappe above the LMMZ. This may record partial recrystallisation of micas due to partitioning of deformation into these less competent units that are within a few kilometers of the LMMZ, which the other weakly deformed units in the hanging wall of the LMMZ escaped.

However, there are several caveats in comparing these literature data with our new data. First, all the ages of Hunziker et al. (1992) are plagued by the fact that they represent bulk K–Ar ages and not stepwise heating analysis. This leaves some uncertainty with respect to the interpretation of the ages, notably it cannot be detected whether these samples contain excess Ar and/or potential inheritance from micas preserved from previous magmatic

or metamorphic events. This would lead to K–Ar ages that are too old, so these should be regarded as maximum ages. Nevertheless, phengite ages from more deformed rocks range from 69 to 61 Ma, broadly consistent with our new rutile age. The same observation can be made for K–Ar ages for phengites from deformed metaradiolarites from the lower Austroalpine Err-nappe, the lateral equivalent of the Margna nappe. There, the phengite ages range from 89 to 67 Ma (Handy et al. 1996). Collectively we propose that K–Ar ages rather represent maximum ages for Alpine metamorphism, and that highly deformed samples best approach the ‘true’ Alpine age, owing to more complete re-equilibration due to deformation-induced recrystallisation of preexisting mica and/or these samples having a greater tendency towards growth of new phengite during Alpine metamorphism. The K–Ar ages from these highly deformed samples approach our new rutile ages.

None of the white mica samples of Price et al. (2018) gave plateau Ar–Ar ages, and instead “integrated” ages were calculated, presumably by averaging some or all of the steps. In some samples a part of the spectrum gave a reasonably coherent age spectrum, albeit not a true plateau, but in other samples extremely heterogeneous age steps cast doubt on the geological meaning of averaging of any of these steps. Above we discussed only their Ar–Ar white mica ages that gave reasonably coherent Ar–Ar spectra for at least part of the analysis, which we infer were the most recrystallised during Alpine metamorphism. However, the fact that even these did not give plateau ages implies that they still retain some inherited component.

The only previous direct geochronological constraints for Alpine metamorphism in the Malenco unit is from Ar–Ar dating of hornblende from three samples of mafic, ultramafic and blackwall lithologies (Villa et al. 2000). In that study, bulk separates of hornblende were dated by Ar–Ar step-heating, which produced complex spectra for all samples, with no plateau ages. Villa et al. (2000) interpreted these spectra as the result of mixing of two to three populations of amphibole of different ages, and used chemical correlation diagrams to extract minimum and maximum ages for the older and younger populations respectively, within each sample. Integrating qualitative pressure constraints from geochemical data for amphiboles, Villa et al. (2000) proposed that early, high pressure Alpine metamorphism in the Malenco unit occurred at 83–91 Ma, while the subsequent temperature-dominated Alpine event occurred at 67–73 Ma. The 83–91 Ma age for the Alpine pressure maximum proposed by Villa et al. (2000) based on their Ar–Ar hornblende ages is resolvably older than our new rutile U–Pb age of 63.0 ± 3.0 Ma; similarly, the 67–73 Ma age for the Alpine thermal maximum (Villa et al. 2000) is also older than our new titanite U–Pb age of 54.7 ± 4.1 Ma.

The younger titanite age is not necessarily in conflict with the Ar–Ar hornblende ages, given that we cannot resolve whether titanite grew during the thermal maximum or subsequent decompression. Amphibole compositions that were related to the temperature-dominated metamorphism record a significant decrease in pressure compared to the earlier population of amphiboles (Villa et al. 2000), but there is no direct evidence that they should have formed precisely at the thermal maximum. However, unless the P–T evolution was more complex than the simple clockwise loop currently assumed, our 63.0 ± 3.0 Ma age for rutile conflicts with the 83–91 Ma age for the Alpine pressure peak proposed by Villa et al. (2000), and to some extent their 67–73 Ma age for the thermal peak, given that rutile is interpreted to have grown during the peak pressure of the Alpine evolution. The Ar–Ar amphibole ages are subject to a number of uncertainties in their interpretation. Chemical correlation diagrams applied to Ar–Ar data are a powerful tool to deconvolute mixed amphibole populations, but the degree to which age populations can be distinguished confidently by this method depends on how distinct they are in terms of chemistry, particularly in terms of the Cl/Ca and Ca/K ratios that are also measured during Ar–Ar analysis. The chemical distinction of different age populations in the samples of Villa et al. (2000) is not always unequivocal, with a large degree of overlap in chemistry in many cases. Another limitation of this method of deconvoluting mixed age populations is that it can only provide a minimum age for the older population, and a maximum age for the younger population. This is due to the fact that it is unlikely that any step of the Ar–Ar spectra records degassing purely of one age component out of the mixed amphibole population. In contrast, our U–Pb ages for rutile and titanite each define a single age population that directly dates the growth of the relevant mineral, which thus each record a single, specific point in the Alpine P–T evolution of the Malenco–Magna area. We therefore consider that our new U–Pb ages for rutile and titanite provide the most reliable geochronological constraints yet for the Alpine evolution in the Malenco region. Interestingly, of the three samples analysed by Villa et al. (2000), the only one in which amphibole was pervasively recrystallised during Alpine metamorphism (their blackwall sample L-F6) gave a ^{39}Ar – ^{40}Ar spectra dominated by steps with 55–65 Ma apparent ages, with apparent ages ≤ 75 Ma for all steps. The ^{39}Ar – ^{40}Ar steps thus cover a remarkably similar age range to that defined by our rutile and titanite ages. Villa et al. (2000) interpreted the ^{39}Ar – ^{40}Ar data for this sample as a complex mixture of three amphibole populations, although from examination of their Fig. 7 the two younger amphibole populations do not appear clearly distinguished in terms of chemistry.

The pressure increase to peak Alpine conditions corresponds to, at the scale of the Central Alps, the nappe stacking and associated pressure-dominated ductile deformation (Mohn et al. 2011), and at a larger scale, is related to subduction. We note that although our 63.0 ± 3.0 Ma age for rutile suggests the occurrence of high pressure conditions later than suggested by previous ^{39}Ar – ^{40}Ar geochronology (Villa et al. 2000), we do not suggest that subduction did not initiate until this time. Turonian (~ 90 Ma) terrigenous flysch sediments deposited on the distal Adriatic margin are preserved in the Southern Alps and record orogenic uplift at this time (Bernoulli and Winkler 1990). Cretaceous terrigenous flysch deposits attributed to orogeny in response to the closure of the Piemonte–Liguria ocean are widespread throughout the Alps, Apennines, Pyrenees, Carpathians and Betic Cordillera (e.g. Marroni et al. 1992; Faupl and Wägrich 1992). The sedimentary record thus provides compelling evidence for widespread orogenic uplift related to convergence from the mid-Cretaceous. Our 63.0 ± 3.0 Ma rutile age clearly postdates the onset of convergence, with decompression occurring later than previously thought, as recorded by our 54.7 ± 4.1 Ma titanite age. Integrating the best available data, we propose that the most reliable geochronological records of Alpine metamorphism support the suggestion of Mohn et al. (2011) that the LMMZ is a major decoupling horizon that separates weakly deformed rocks in the hangingwall from strongly deformed rocks in the footwall. The major activity is in the Paleocene to lower Eocene, considerably younger than previous estimates. We do not see any reliable evidence for a ~ 90 Ma event throughout the entire region.

6.6 U–Pb geochronology of rutile and titanite as a valuable tool for dating young, low-grade metamorphic events

The analysed rutiles and titanites were challenging to date, owing to their low U contents, young age, and high proportions of common Pb. U-bearing minerals grown in young metamorphic (or igneous) events have undergone radioactive decay of U for only a short time, and so inevitably have low concentrations of radiogenic Pb, especially given the extremely long half-lives of both U isotopes utilised in geochronology (0.7 and 4.5 Ga; Jaffey et al. 1971; Mattinson 2010). As the amount of radiogenic Pb produced is proportional to the concentration of the parent isotope in the mineral of interest, the problem of low levels of radiogenic Pb is exacerbated if the target grains have low U contents. Although titanite can incorporate tens to thousands of ppm U (e.g. Frost et al. 2001; Stearns et al. 2016; Garber et al. 2017), it can also have extremely low U contents, with low-grade metabasites particularly

challenging for geochronology due to low ratios of U to common Pb (e.g. Frost et al. 2001; Kohn and Corrie 2011). Because titanite has a strong affinity for Pb, it typically takes up appreciable quantities of common Pb, further complicating geochronology (e.g. Frost et al. 2001; Marsh and Smye 2017; Kohn 2017; Kirkland et al. 2018). Rutile usually has low concentrations of common Pb, but also tends to have lower U concentrations than titanite, particularly in metabasic rocks of which > 60% from a recent compilation have rutile with < 4 ppm U (Zack and Kooijman 2017).

The Alpine titanites analysed in this study have rather low U contents (4–58 ppm U, with an average of 22 ppm), which together with their young age results in very low radiogenic Pb (Pb^*) concentrations. This, combined with significant absolute concentrations of common Pb (Pb_C), results in extremely high Pb_C/Pb^* for the titanites. Their ^{206}Pb concentrations range only from 0.2 to 3.0 ppm, with an average of 0.9 ppm. This ^{206}Pb is a mixture of radiogenic and common, with ubiquitously high common Pb contents. Thus, of the low quantities of Pb to be measured, a large proportion must be stripped to correct for the common Pb contribution, in order to calculate the much lower quantities of radiogenic Pb. This makes accurately constraining the radiogenic Pb concentrations, and therefore age, of these titanites particularly challenging. Our analysed rutiles have even lower U contents of 0.3–12 ppm, with sample averages of only 4–6 ppm U, and average ^{206}Pb concentrations of only 0.06–0.1 ppm. Although the rutiles contain low absolute concentrations of Pb_C , and have lower Pb_C/Pb^* than the titanites (Figs. 5, 6), a significant proportion of the small signal on ^{206}Pb still has to be stripped to correct for the contribution of common Pb in rutile.

We have shown here that, in spite of these challenges, it is possible to date these young, low-grade, low-U rutiles and titanites accurately and relatively precisely. The approach of using a 2-dimensional isochron without a fixed upper intercept has long been recognised as a particularly robust method of common Pb correction for high-common Pb minerals such as our titanites, as it takes advantage of the wide range of Pb_C/Pb^* up to high values, resulting from the between-grain range in U content, to yield a very well-constrained isochron without the need to fix a common Pb composition (e.g. Ludwig 1998; Frost et al. 2001; Storey et al. 2006; Chew et al. 2014; Stearns et al. 2016; Kohn 2017). Inferring the common Pb composition from the data themselves, rather than making assumptions about the common Pb composition, is particularly advantageous in a relatively low-temperature setting such as experienced by the Ur breccia during Alpine metamorphism. Independent determinations of common Pb composition normally either assume a model common Pb composition based on the time

at which it was thought to be incorporated (e.g. Stacey and Kramers 1975), or use a measurement of the isotopic composition of Pb for a mineral from the same sample that is low in U and thought to have been in equilibrium with the dated mineral at the relevant time. In low-temperature metamorphic settings the length-scales on which chemical equilibrium is expected reduce dramatically, and the assumption that co-existing minerals in the same hand specimen are likely to be in equilibrium breaks down (e.g. Cruz-Uribe et al. 2018). This approach would be particularly dangerous in our samples, which are highly heterogeneous breccias. Whether or not a given mineral has re-equilibrated its Pb isotopic composition will also depend on the closure temperature of Pb in that mineral. It is not obvious which mineral, if any, would be an appropriate proxy for the common Pb composition of the rutile and titanite in these samples. The approach of independently constraining the common Pb composition from isochron data has previously been shown to be particularly valuable for titanite, as it can sometimes incorporate initial Pb with compositions far removed from age-dependent model Pb compositions, particularly when it has been inherited from the breakdown of U-rich precursor phases during metamorphic reactions (e.g. Romer and Rötzler 2003; Marsh and Smye 2017; Kirkland et al. 2017, 2018). In such cases different grains of titanite in the same sample can inherit distinctly different initial Pb compositions (Essex and Gromet 2000; Kohn 2017). Importantly, the fit of the data to a two-dimensional isochron, as quantified by the MSWD, can be used to test the validity of using the same common Pb composition for all analysed titanites. In the case of our samples, the $^{207}Pb/^{206}Pb_{\text{common}}$ determined from isochrons was always within error of the model common Pb composition for 60 Ma (Stacey and Kramers 1975) for both rutile and titanite. Although in this case a model common Pb composition would, in fact, have been appropriate, it is crucial to have confirmed this assumption from the data themselves. Furthermore, in the case of the titanites, the $^{207}Pb/^{206}Pb_{\text{common}}$ is actually more precisely constrained from the isochron for the pooled data for all samples than from the Stacey–Kramers model composition (Fig. 5), making the common Pb composition determined from the unanchored isochron the preferred choice. For the rutiles, the $^{207}Pb/^{206}Pb_{\text{common}}$ was determined much less precisely from the isochrons, making an isochron anchored to the Stacey–Kramers model composition for 60 Ma the preferred method of age determination. This choice is placed on firm footing by the evidence from the $^{207}Pb/^{206}Pb_{\text{common}}$ calculated from unanchored isochrons that this common Pb composition is appropriate for rutile in these samples.

For young rutiles and titanites like those dated here, the low concentrations of Pb are the biggest limiting factor

analytically. All isotopes of Pb are present at very low concentrations, making the measured $^{207}\text{Pb}/^{206}\text{Pb}$ extremely imprecise. Although U concentrations are also low, they are still an order of magnitude higher than Pb. This makes the modification of the traditional two-dimensional isochron that we have presented here particularly valuable in young samples like ours, as the use of a Wetherill (rather than Tera-Wasserburg) concordia diagram to regress the data allows the most precise input ratios to be used to constrain the isochron. For samples with high proportions of common Pb, the alternative approach of calculating the $^{207}\text{Pb}/^{206}\text{Pb}$ from the more precisely-measured Wetherill ratios to allow plotting on a Tera-Wasserburg concordia necessitates the laborious conversion of isotope ratios, uncertainties and error correlations by hand following a series of equations (Ludwig 2012). The approach of using a Wetherill concordia to determine both isochron ages and common Pb composition allows plotting of the ratios directly as measured and thus provides a simplified method to obtain more precise isochron ages from young, low-U minerals, improving the applicability of in situ U–Pb geochronology of minerals such as titanite to date young, low-grade metamorphic events. The traditional Tera-Wasserburg isochron retains the advantage that the common Pb composition is more immediately obvious visually, but in cases where improved precision justifies the use of a Wetherill concordia (as for our titanites), this disadvantage can easily be overcome by calculation of $^{207}\text{Pb}/^{206}\text{Pb}_{\text{common}}$ from the slope of the isochron. For isochrons with relatively low Pb_C/Pb^* and/or insufficient spread in Pb_C/Pb^* , age precision may be improved by using a model or independently-determined common Pb composition. In this case the Tera-Wasserburg with measured $^{207}\text{Pb}/^{206}\text{Pb}$ is the concordia of choice, as it is the only option that allows anchoring of the isochron to a specific $^{207}\text{Pb}/^{206}\text{Pb}_{\text{common}}$.

In the case of titanite, a key advantage for dating low-grade events is its high closure temperature, which means that if it grew during moderate- to low-grade metamorphism its U/Pb is expected to record a growth age. This significantly simplifies interpretation of the age, as it means precise knowledge of the closure temperature is not required, and allows direct dating of the metamorphic reaction that produced titanite. Titanite reacts readily during metamorphism (e.g. Frost et al. 2001; Bonamici et al. 2015; Kirkland et al. 2016; Garber et al. 2017; Kohn 2017), and its stability for a given bulk composition can be related to pressure and temperature conditions, making it well-placed to record such moderate-temperature metamorphism.

7 Conclusions

We performed in situ U–Pb dating on rutile and titanite in the region of Val Malenco in the eastern Central Alps. Both accessory minerals are encountered in tectonised units comprised between the Margna continental crust nappe and Malenco serpentinitized peridotites. These units are made of brecciated material of both continental crust and upper mantle as well as metasomatic rocks (blackwalls) at the contact with mantle rocks. Rutile and titanite formed in the whole section from breccia to blackwall. It has been described that titanite overgrew rutile from the metamorphic reaction $\text{rutile} + \text{epidote} + \text{quartz} \rightarrow \text{titanite} + \text{anorthite} + \text{water}$. As rutile and titanite relate to the high pressure and temperature parts of the Alpine evolution respectively, dating both minerals gives important constraints on the timing of different Alpine metamorphic conditions and metamorphic reactions. As the Malenco region underwent metamorphism that did not exceed $460 \pm 30^\circ\text{C}$, which is below the closure temperature (T_C) of Pb in both rutile and titanite, we thus date their crystallisation ages during Alpine metamorphism. Rutile and titanite have low U and radiogenic Pb (Pb^*), and high and variable ratios of common Pb to radiogenic Pb. We have shown that for titanite from our samples, the best age constraints are obtained using an unanchored isochron lower intercept age calculated on a Wetherill concordia, which allows the use of the most precise input ratios available, while avoiding the need to recalculate ratios, uncertainties and error correlations to allow plotting on a Tera-Wasserburg diagram. Both isochron ages and the composition of common Pb are determined more precisely for these titanites on a Wetherill concordia compared to the traditional Tera-Wasserburg concordia with measured ratios. This demonstrates the value of this approach for young, low U and high Pb_C/Pb^* minerals. For rutiles from our samples, lower and less variable Pb_C/Pb^* result in common Pb compositions being imprecisely determined from isochrons, and lower intercept age precision was significantly improved by anchoring isochrons to a model common Pb composition, necessitating the use of a Tera-Wasserburg concordia for rutiles. Ages obtained are 63.0 ± 3.0 Ma for rutile and 54.7 ± 4.1 Ma for titanite. The rutile age corresponds to elevated pressure metamorphism associated with nappe stacking. Titanite ages likely date peak temperature during Alpine metamorphism. An analysis of available Rb–Sr, K–Ar and Ar–Ar ages for the wider region from the literature are in broad agreement with our age range and indicates a Paleocene to lower Eocene age of metamorphic recrystallization, constraining the activity along and below the Lunghin–Mortirolo movement zone. Further studies that precisely date

foliations above and below the Lunghin–Mortirolo movement zone could test whether the proposed Paleocene (instead of Cretaceous) age of metamorphism is widespread. If so, the timing of the geological evolution of the Pennine Austroalpine boundary in the eastern Central Alps and its tectonic implications need to be seriously revised.

Acknowledgements We are particularly thankful to Peter Zwahlen from the Büro für Technische Geologie (BTG) in Chur for providing the drillcores for our research. We thank Alexey Ulianov for his dedicated assistance during LA-ICPMS analysis, and Jörg Hermann for stimulating discussions. We are grateful to reviewers Andrew Kylander-Clark and Geoffroy Mohn for their insightful comments that helped to significantly improve the manuscript, and to Edwin Gnos for editorial handling. We thank Tim Raupach for writing for us the R script to simulate longer dwell times by averaging five integrations together.

Open Access This article is distributed under the terms of the Creative Commons Attribution 4.0 International License (<http://creativecommons.org/licenses/by/4.0/>), which permits unrestricted use, distribution, and reproduction in any medium, provided you give appropriate credit to the original author(s) and the source, provide a link to the Creative Commons license, and indicate if changes were made.

References

- Andersen, T. (2002). Correction of common lead in U–Pb analyses that do not report ^{204}Pb . *Chemical Geology*, 192(1–2), 59–79.
- Bachmann, R., Glodny, J., Oncken, O., & Seifert, W. (2009). Abandonment of the South Penninic–Austroalpine palaeosubduction zone, Central Alps, and shift from subduction erosion to accretion: constraints from Rb/Sr geochronology. *Journal of the Geological Society, London*, 166, 217–231. <https://doi.org/10.1144/0016-76492008-024>.
- Beltrando, M., Manatschal, G., Mohn, G., Dal Piaz, G. V., Brovarone, A. V., & Masini, E. (2014). Recognizing remnants of magma-poor rifted margins in high-pressure orogenic belts: The Alpine case study. *Earth-Science Reviews*, 131, 88–115.
- Benning, L. G., & Sidler, D. (1992). Petrographie der Margna- und der Sella-Decke und des Malenco-Serpentinities zwischen Pass d’Ur und Pizzo Scalino (Val Malenco, Provinz Sondrio, Italien). *Schweizerische Mineralogische und Petrographische Mitteilungen*, 72, 213–224.
- Bernoulli, D., & Winkler, W. (1990). Heavy mineral assemblages from Upper Cretaceous South- and Austroalpine flysch sequences (Northern Italy and Southern Switzerland): source terranes and palaeotectonic implications. *Eclogae Geologicae Helveticae*, 83(2), 287–310.
- Bohlen, S. R., & Liotta, J. J. (1986). A barometer for garnet amphibolites and garnet granulites. *Journal of Petrology*, 27(5), 1025–1034.
- Bohlen, S. R., Wall, V. J., & Boettcher, A. L. (1983). Experimental investigations and geological applications of equilibria in the system $\text{FeO-TiO}_2\text{-Al}_2\text{O}_3\text{-SiO}_2\text{-H}_2\text{O}$. *American Mineralogist*, 68, 1049–1058.
- Bonamici, C. E., Fanning, C. M., Kozdon, R., Fournelle, J. H., & Valley, J. W. (2015). Combined oxygen-isotope and U–Pb zoning studies of titanite: New criteria for age preservation. *Chemical Geology*, 398, 70–84.
- Cherniak, D. J. (1993). Lead diffusion in titanite and preliminary results on the effects of radiation damage on Pb transport. *Chemical Geology*, 110(1–3), 177–194.
- Cherniak, D. J. (2000). Pb diffusion in rutile. *Contributions to Mineralogy and Petrology*, 139(2), 198–207.
- Chew, D. M., Petrus, J. A., & Kamber, B. S. (2014). U–Pb LA-ICPMS dating using accessory mineral standards with variable common Pb. *Chemical Geology*, 363, 185–199.
- Cruz-Uribe, A. M., Feineman, M. D., Zack, T., & Barth, M. (2014). Metamorphic reaction rates at $\sim 650\text{--}800^\circ\text{C}$ from diffusion of niobium in rutile. *Geochimica et Cosmochimica Acta*, 130, 63–77.
- Cruz-Uribe, A. M., Feineman, M. D., Zack, T., & Jacob, D. E. (2018). Assessing trace element (dis)equilibrium and the application of single element thermometers in metamorphic rocks. *Lithos*, 314–315, 1–15.
- Engi, M. (2017). Petrochronology based on REE-minerals: monazite, allanite, xenotime, apatite. *Reviews in Mineralogy and Geochemistry*, 83(1), 365–418.
- Ernst, W. G., & Liu, J. (1998). Experimental phase-equilibrium study of Al- and Ti-contents of calcic amphibole in MORB—a semiquantitative thermobarometer. *American Mineralogist*, 83, 952–969.
- Essex, R. M., & Gromet, L. P. (2000). U–Pb dating of prograde and retrograde titanite growth during the Scandian orogeny. *Geology*, 28(5), 419–422.
- Ewing, T. E. (2011). Hf isotope analysis and U–Pb geochronology of rutile: Technique development and application to a lower crustal section (Ivrea–Verbano Zone, Italy). *Unpublished PhD thesis*. Australian National University.
- Faupl, P., & Wagerich, M. (1992). Cretaceous flysch and pelagic sequences of the Eastern Alps: Correlations, heavy minerals, and palaeogeographic implications. *Cretaceous Research*, 13(5), 387–403.
- Ferry, J. M., & Watson, E. B. (2007). New thermodynamic models and revised calibrations for the Ti-in-zircon and Zr-in-rutile thermometers. *Contributions to Mineralogy and Petrology*, 154(4), 429–437.
- Froitzheim, N., & Eberli, G. P. (1990). Extensional faulting in the evolution of a Tethys passive continental margin, Eastern Alps, Switzerland. *Geological Society of America Bulletin*, 102(9), 1297–1308.
- Froitzheim, N., & Manatschal, G. (1996). Kinematics of Jurassic rifting, mantle exhumation, and passive-margin formation in the Austroalpine and Penninic nappes (eastern Switzerland). *Geological Society of America Bulletin*, 108(9), 1120–1133.
- Froitzheim, N., Schmid, S. M., & Conti, P. (1994). Repeated change from crustal shortening to orogen-parallel extension in the Austroalpine units of Graubünden. *Eclogae Geologicae Helveticae*, 87, 559–612.
- Frost, R. (1975). Contact metamorphism of serpentinite, chloritic blackwall and rodingite at Paddy-Go-Easy Pass, Central Cascades, Washington. *Journal of Petrology*, 16(2), 272–313.
- Frost, B. R., Chamberlain, K. R., & Schumacher, J. C. (2001). Sphene (titanite): Phase relations and role as a geochronometer. *Chemical Geology*, 172(1), 131–148.
- Gao, X. Y., Zheng, Y. F., Chen, Y. X., & Guo, J. (2012). Geochemical and U–Pb age constraints on the occurrence of polygenetic titanites in UHP metagranite in the Dabie orogen. *Lithos*, 136, 93–108.
- Garber, J. M., Hacker, B. R., Kylander-Clark, A. R. C., Stearns, M., & Seward, G. (2017). Controls on trace element uptake in metamorphic titanite: Implications for petrochronology. *Journal of Petrology*, 58(6), 1031–1057.
- Gerdes, A., & Zeh, A. (2006). Combined U–Pb and Hf isotope LA-(MC-) ICP-MS analyses of detrital zircons: comparison with

- SHRIMP and new constraints for the provenance and age of an Armorican metasediment in Central Germany. *Earth and Planetary Science Letters*, 249(1–2), 47–61.
- Guntli, P., & Liniger, M. (1989). Metamorphose in der Margna-Decke im Bereich Piz da la Margna und Piz Fedoz (Oberengadin). *Schweizerische Mineralogische und Petrographische Mitteilungen*, 69(2), 289–301.
- Handy, M. R., Herwegh, M., Kamber, B., Tietz, R., & Villa, I. M. (1996). Geochronologic, petrologic and kinematic constraints on the evolution of the Err-Platta boundary, part of a fossil continent-ocean suture in the Alps (eastern Switzerland). *Schweizerische Mineralogische und Petrographische Mitteilungen*, 76(3), 453–474.
- Hayden, L. A., Watson, E. B., & Wark, D. A. (2008). A thermobarometer for sphene (titanite). *Contributions to Mineralogy and Petrology*, 155(4), 529–540.
- Hermann, J., & Müntener, O. (1996). Extension-related structures in the Malenco–Margna-system: Implications for paleogeography and consequences for rifting and Alpine tectonics. *Schweizerische Mineralogische und Petrographische Mitteilungen*, 76(3), 501–520.
- Hiess, J., Condon, D. J., McLean, N., & Noble, S. R. (2012). $^{238}\text{U}/^{235}\text{U}$ systematics in terrestrial uranium-bearing minerals. *Science*, 335(6076), 1610–1614.
- Holder, R. M., Hacker, B. R., Seward, G. G. E., & Kylander-Clark, A. R. C. (2019). Interpreting titanite U–Pb dates and Zr thermobarometry in high-grade rocks: empirical constraints on elemental diffusivities of Pb, Al, Fe, Zr, Nb, and Ce. *Contributions to Mineralogy and Petrology*, 174(5), 42.
- Horn, I., Rudnick, R. L., & McDonough, W. F. (2000). Precise elemental and isotope ratio determination by simultaneous solution nebulization and laser ablation-ICP-MS: Application to U–Pb geochronology. *Chemical Geology*, 164(3–4), 281–301.
- Horstwood, M. S. A., Košler, J., Gehrels, G., Jackson, S. E., McLean, N. M., Paton, C., et al. (2016). Community-derived standards for LA-ICP-MS U–(Th)–Pb geochronology—uncertainty propagation, age interpretation and data reporting. *Geostandards and Geoanalytical Research*, 40, 311–332.
- Hunziker, J., Desmons, J., & Hurford, A. J. (1992). Thirty-two years of geochronological work in the Central and Western Alps—a review on 7 maps. *Mémoires de Géologie (Lausanne)*, 13, 1–64.
- Jaffey, A. H., Flynn, K. F., Glendenin, L. E., Bentley, W. C., & Essling, A. M. (1971). Precision measurement of half-lives and specific activities of ^{235}U and ^{238}U . *Physical Review C*, 4(5), 1889–1906.
- Jochum, K. P., Weis, U., Stoll, B., Kuzmin, D., Yang, Q., Raczek, I., et al. (2011). Determination of reference values for NIST SRM 610–617 glasses following ISO guidelines. *Geostandards and Geoanalytical Research*, 35(4), 397–429.
- Kapp, P., Manning, C. E., & Tropper, P. (2009). Phase-equilibrium constraints on titanite and rutile activities in mafic epidote amphibolites and geobarometry using titanite–rutile equilibria. *Journal of Metamorphic Geology*, 27(7), 509–521.
- Kennedy, A. K., Kamo, S. L., Nasdala, L., & Timms, N. E. (2010). Grenville skarn titanite: potential reference material for SIMS U–Th–Pb analysis. *The Canadian Mineralogist*, 48, 1423–1443.
- Kirkland, C. L., Fougereuse, D., Reddy, S. M., Hollis, J., & Saxey, D. W. (2018). Assessing the mechanisms of common Pb incorporation into titanite. *Chemical Geology*, 483, 558–566.
- Kirkland, C. L., Hollis, J., Danišik, M., Petersen, J., Evans, N. J., & McDonald, B. J. (2017). Apatite and titanite from the Karrat Group, Greenland; implications for charting the thermal evolution of crust from the U–Pb geochronology of common Pb bearing phases. *Precambrian Research*, 300, 107–120.
- Kirkland, C. L., Spaggiari, C. V., Johnson, T. E., Smithies, R. H., Danišik, M., Evans, N., et al. (2016). Grain size matters: Implications for element and isotopic mobility in titanite. *Precambrian Research*, 278, 283–302.
- Kohn, M. J. (2017). Titanite petrochronology. *Reviews in Mineralogy and Geochemistry*, 83(1), 419–441.
- Kohn, M. J., & Corrie, S. L. (2011). Preserved Zr-temperatures and U–Pb ages in high-grade metamorphic titanite: Evidence for a static hot channel in the Himalayan orogen. *Earth and Planetary Science Letters*, 311(1–2), 136–143.
- Kooijman, E., Mezger, K., & Berndt, J. (2010). Constraints on the U–Pb systematics of metamorphic rutile from in situ LA-ICP-MS analysis. *Earth and Planetary Science Letters*, 293(3–4), 321–330.
- Lemoine, M., & Trümpy, R. (1987). Pre-oceanic rifting in the Alps. *Tectonophysics*, 133(3–4), 305–320.
- Liu, J., Bohlen, S. R., & Ernst, W. G. (1996). Stability of hydrous phases in subducting oceanic crust. *Earth and Planetary Science Letters*, 143, 161–171.
- Locatelli, M., Verlaquet, A., Agard, P., Federico, B., & Angiboust, S. (2018). Intermediate-depth brecciation along the subduction plate interface (Monviso eclogite, W. Alps). *Lithos*, 320/321, 378–402.
- Lucassen, F., Dulski, P., Abart, R., Franz, G., Rhede, D., & Romer, R. L. (2010). Redistribution of HFSE elements during rutile replacement by titanite. *Contributions to Mineralogy and Petrology*, 160(2), 279–295.
- Ludwig, K. (1998). On the treatment of concordant uranium-lead ages. *Geochimica et Cosmochimica Acta*, 62, 665–676.
- Ludwig, K. R. (2012). User's manual for Isoplot 3.75: A geochronological toolkit for microsoft excel. In *Berkeley Geochronology Center Special Publication No. 5*.
- Luvizotto, G., Zack, T., Meyer, H., Ludwig, T., Triebold, S., Kronz, A., et al. (2009). Rutile crystals as potential trace element and isotope mineral standards for microanalysis. *Chemical Geology*, 261, 346–369.
- Manatschal, G., & Müntener, O. (2009). A type sequence across an ancient magma-poor ocean–continent transition: the example of the western Alpine Tethys ophiolites. *Tectonophysics*, 473(1–2), 4–19.
- Marroni, M., Monechi, S., Perilli, N., Principi, G., & Treves, B. (1992). Late Cretaceous flysch deposits of the Northern Apennines, Italy: Age of inception of orogenesis-controlled sedimentation. *Cretaceous Research*, 13(5–6), 487–504.
- Marsh, J. H., & Smye, A. J. (2017). U–Pb systematics and trace element characteristics in titanite from a high-pressure mafic granulite. *Chemical Geology*, 466, 403–416.
- Masini, E., Manatschal, G., Mohn, G., & Unternehr, P. (2012). Anatomy and tectono-sedimentary evolution of a rift-related detachment system: The example of the Err detachment (central Alps, SE Switzerland). *Geological Society of America Bulletin*, 124(9–10), 1535–1551.
- Masson, H., Bussy, F., Eichenberger, M., Giroud, N., Meilhac, C., & Presniakov, S. (2008). Early Carboniferous age of the Versoyen ophiolites and consequences: non-existence of a “Valais ocean” (Lower Penninic, western Alps). *Bulletin de la Société Géologique de France*, 179(4), 337–355.
- Mattinson, J. M. (1978). Age, origin, and thermal histories of some plutonic rocks from the Salinian block of California. *Contributions to Mineralogy and Petrology*, 67(3), 233–245.
- Mattinson, J. M. (2010). Analysis of the relative decay constants of ^{235}U and ^{238}U by multi-step CA-TIMS measurements of closed-system natural zircon samples. *Chemical Geology*, 275(3), 186–198.
- Mellini, M., Trommsdorff, V., & Compagnoni, R. (1987). Antigorite polysomatism: Behaviour during progressive metasomatism. *Contributions to Mineralogy and Petrology*, 97, 147–155.

- Mezger, K., Hanson, G., & Bohlen, S. (1989). High-precision U–Pb ages of metamorphic rutile: Application to the cooling history of high-grade terranes. *Earth Planetary Science Letters*, 96, 106–118.
- Mohn, G., Manatschal, G., Masini, E., & Müntener, O. (2011). Rift-related inheritance in orogens: A case study from the Austroalpine nappes in Central Alps (SE-Switzerland and N-Italy). *International Journal of Earth Sciences*, 100(5), 937–961.
- Mohn, G., Manatschal, G., Müntener, O., Beltrando, M., & Masini, E. (2010). Unravelling the interaction between tectonic and sedimentary processes during lithospheric thinning in the Alpine Tethys margins. *International Journal of Earth Sciences*, 99(1), 75–101.
- Montrasio, A., Trommsdorff, V., Hermann, J., Müntener, O., & Spillmann, P. (2005). Carta geologica della Valmalenco. *Supplement to Schweizerische Mineralogische und Petrographische Mitteilungen*, 85(1).
- Müntener, O., & Hermann, J. (1996). The Val Malenco lower crust—upper mantle complex and its field relations (Italian Alps). *Schweizerische Mineralogische und Petrographische Mitteilungen*, 76, 475–500.
- Müntener, O., Hermann, J., & Trommsdorff, V. (2000). Cooling history and exhumation of lower-crustal granulite and upper mantle (Malenco, Eastern Central Alps). *Journal of Petrology*, 41(2), 175–200.
- Nievergelt, P., Liniger, M., Froitzheim, N., & Mählmann, R. F. (1996). Early to mid tertiary crustal extension in the Central Alps: The Turba mylonite zone (Eastern Switzerland). *Tectonics*, 15, 329–340.
- Paton, C., Hellstrom, J., Paul, B., Woodhead, J., & Hergt, J. (2011). Iolite: Freeware for the visualisation and processing of mass spectrometric data. *Journal of Analytical Atomic Spectrometry*, 26, 2508–2518.
- Paton, C., Woodhead, J. D., Hellstrom, J. C., Hergt, J. M., Greig, A., & Maas, R. (2010). Improved laser ablation U–Pb zircon geochronology through robust downhole fractionation correction. *Geochemistry, Geophysics, Geosystems*, 11, Q0AA06.
- Petrus, J. A., & Kamber, B. S. (2012). VizualAge: A novel approach to laser ablation ICP-MS U–Pb geochronology data reduction. *Geostandards and Geoanalytical Research*, 36(3), 247–270.
- Picazo, S., Manatschal, G., Cannat, M., & Andréani, M. (2013). Deformation associated to exhumation of serpentinized mantle rocks in a fossil ocean continent transition: The Totalp unit in SE Switzerland. *Lithos*, 175, 255–271.
- Picazo, S., Müntener, O., Manatschal, G., Bauville, A., Karner, G., & Johnson, C. (2016). Mapping the mantle domains in Western and Central Europe based on clinopyroxene and spinel chemistry: Evidence for mantle modification during an extensional cycle. *Lithos*, 266–267, 233–263.
- Pozzorini, D. (1996). Stable isotope investigations of ophicarbonate rocks, Bergell Aureole, Valmalenco: Constraints on fluid–rock interaction. *Doctoral dissertation*, ETH Zurich.
- Price, J. B., Wernicke, B. P., Cosca, M. A., & Farley, K. A. (2018). Thermochronometry across the Austroalpine–Pennine Boundary, Central Alps, Switzerland: Orogen-perpendicular normal fault slip on a major “overthrust” and its implications for orogenesis. *Tectonics*, 37(3), 724–757.
- Rasmussen, B., Fletcher, I. R., & McNaughton, N. J. (2001). Dating low-grade metamorphic events by SHRIMP U–Pb analysis of monazite in shales. *Geology*, 29(10), 963–966.
- Romer, R. L., & Rötzler, J. (2003). Effect of metamorphic reaction history on the U–Pb dating of titanite. *Geological Society, London, Special Publications*, 220(1), 147–158.
- Rubatto, D. (2017). Zircon the metamorphic mineral. *Reviews in Mineralogy and Geochemistry*, 83(1), 261–295.
- Schmid, S. M., Fügenschuh, B., Kissling, E., & Schuster, R. (2004). Tectonic map and overall architecture of the Alpine orogen. *Eclogae Geologicae Helveticae*, 97, 93–117. <https://doi.org/10.1007/s00015-004-1113-x>.
- Scott, D. J., & St-Onge, M. R. (1995). Constraints on Pb closure temperature in titanite based on rocks from the Ungava orogen, Canada: Implications for U–Pb geochronology and PTt path determinations. *Geology*, 23(12), 1123–1126.
- Sidler, D. M., & Benning, L. G. (1992). Die Entwicklung der Strukturen im Südosten der Margna-Decke und des Malenco-Ultramafits (Provinz Sondrio, Italien). Structures in the South-eastern Margna nappe and in the Malenco ultramafite (Province Sondrio, Italy). *Schweizerische Mineralogische und Petrographische Mitteilungen*, 72, 57–68.
- Siegesmund, S., Layer, P., Dunkl, I., Vollbrecht, A., Steenken, A., Wemmer, K., & Ahrendt, H. (2008). Exhumation and deformation history of the lower crustal section of the Valstrona di Omegna in the Ivrea Zone, southern Alps. Tectonic Aspects of the Alpine-Dinaride-Carpathian System.
- Spandler, C., Hammerli, J., Sha, P., Hilbert-Wolf, H., Hu, Y., Roberts, E., et al. (2016). MKED1: A new titanite standard for in situ analysis of Sm–Nd isotopes and U–Pb geochronology. *Chemical Geology*, 425, 110–126.
- Spencer, K. J., Hacker, B. R., Kylander-Clark, A. R. C., Andersen, T. B., Cottle, J. M., Stearns, M. A., et al. (2013). Campaign-style titanite U–Pb dating by laser-ablation ICP: Implications for crustal flow, phase transformations and titanite closure. *Chemical Geology*, 341, 84–101.
- Spillmann, P., & Büchi, H. J. (1993). The pre-Alpine basement of the lower Austro-Alpine Nappes in the Bernina massif (Grisons, Switzerland; Valtellina, Italy). In J. F. von Raumer & F. Neubauer (Eds.), *Pre-mesozoic geology alps* (pp. 457–467). Heidelberg: Springer.
- Stacey, J. S., & Kramers, J. D. (1975). Approximation of terrestrial lead isotope evolution by a two-stage model. *Earth and Planetary Science Letters*, 26, 207–221.
- Stearns, M. A., Cottle, J. M., Hacker, B. R., & Kylander-Clark, A. R. C. (2016). Extracting thermal histories from the near-rim zoning in titanite using coupled U–Pb and trace-element depth profiles by single-shot laser-ablation split stream (SS-LASS) ICP-MS. *Chemical Geology*, 422, 13–24.
- Storey, C. D., Jeffries, T. E., & Smith, M. (2006). Common lead-corrected laser ablation ICP-MS U–Pb systematics and geochronology of titanite. *Chemical Geology*, 227(1–2), 37–52.
- Tera, F., & Wasserburg, J. (1972). U–Th–Pb systematics in three Apollo 14 basalts and the problem of initial Pb in lunar rocks. *Earth and Planetary Science Letters*, 14, 281–304.
- Tomkins, H. S., Powell, R., & Ellis, D. J. (2007). The pressure dependence of the zirconium-in-rutile thermometer. *Journal of Metamorphic Geology*, 25(6), 703–713.
- Trommsdorff, V., & Evans, B. W. (1972). Progressive metamorphism of antigorite schist in the Bergell tonalite aureole (Italy). *American Journal of Science*, 272(5), 423–437.
- Trommsdorff, V., Piccardo, G. B., & Montrasio, A. (1993). From magmatism through metamorphism to sea floor emplacement of subcontinental Adria lithosphere during pre-Alpine rifting (Malenco, Italy). *Schweizerische Mineralogische und Petrographische Mitteilungen*, 73(2), 191–203.
- Ulmer, P., & Trommsdorff, V. (1999). Phase relations of hydrous mantle subducting to 300 km. In Y. Fei, C. M. Bertka, & B. O. Mysen (Eds.), *Mantle Petrology: Field Observations and High Pressure Experimentation: A Tribute to Francis R. (Joe) Boyd*. (pp. 259–281). Geochem. Soc. Spec. Publ. 6.
- Villa, I. M., Hermann, J., Müntener, O., & Trommsdorff, V. (2000). ³⁹Ar–⁴⁰Ar dating of multiply zoned amphibole generations

- (Malenco, Italian Alps). *Contributions to Mineralogy and Petrology*, 140, 363–381.
- Vry, J. K., & Baker, J. A. (2006). LA-MC-ICPMS Pb–Pb dating of rutile from slowly cooled granulites: confirmation of the high closure temperature for Pb diffusion in rutile. *Geochimica Cosmochimica Acta*, 70, 1807–1820.
- Warren, C. J., Grujic, D., Cottle, J. M., & Rogers, N. W. (2012). Constraining cooling histories: Rutile and titanite chronology and diffusion modelling in NW Bhutan. *Journal of Metamorphic Geology*, 30(2), 113–130.
- Watson, E. B., Wark, D. A., & Thomas, J. B. (2006). Crystallization thermometers for zircon and rutile. *Contributions to Mineralogy and Petrology*, 151(4), 413–433.
- Zack, T., Cruz-Urbe, A., & Barth, M. G. (2010). Dating metasomatism: U/Pb ages of titanite overgrowth on rutile from the Catalina Schist migmatites, Catalina Island. In *AGU Fall Meeting abstracts*.
- Zack, T., & Kooijman, E. (2017). Petrology and geochronology of rutile. *Reviews in Mineralogy and Geochemistry*, 83(1), 443–467.
- Zack, T., Moraes, R., & Kronz, A. (2004). Temperature dependence of Zr in rutile: Empirical calibration of a rutile thermometer. *Contributions to Mineralogy and Petrology*, 148, 471–488.
- Zack, T., Stockli, D. F., Luvizotto, G. L., Barth, M. G., Belousova, E., Wolfe, M. R., et al. (2011). In situ U–Pb rutile dating by LA-ICP-MS: 208Pb correction and prospects for geological applications. *Contributions to Mineralogy and Petrology*, 162, 515–530.